Nrf2- and ATF4-Dependent Upregulation of xCT Modulates the Sensitivity of T24 Bladder Carcinoma Cells to Proteasome Inhibition

（Nrf2 と ATF4 依存的な xCT 誘導による T24 膀胱癌細胞のプロテアソーム阻害に対する感受性の制御）

申　請　者　　弘前大学大学院医学研究科
病態制御科学領域
分子生体防御学教育研究分野

氏　名　　叶　鵬

指導教授　　伊東　健

Table of Contents

Abbreviations

AARE; amino acid response element
ARE; antioxidant responsive element
ATF4; activating transcription factor 4
BSA; bovine serum albumin
BTZ; bortezomib
bZip; basic leucine zipper
CFZ; carfilzomib
ChIP; chromatin immunoprecipitation
CNC; Cap'n'Color
CPG; (*S*)-4-carboxyphenylglycine
CypA; cyclophilin A
DMSO; dimethyl sulfoxide
eIF2α; eukaryotic initiation factor 2α
EPO; epoxomicin
ER; endoplasmic reticulum
GSH; glutathione
GST; glutathione *S*-transferase
GCLC; glutamate-cysteine ligase catalytic subunit
GCLM; glutamate-cysteine ligase modulatory subunit
HO-1; heme oxygenase 1
Keap1; kelch-like ECH-associated protein 1
2-ME; 2-mercaptoethanol
NAC; *N*-Acetyl-L-cysteine
Nrf2; NF-E2-related factor 2
PBS; phosphate buffered saline
RT-qPCR; quantitative RT-PCR
SASP; sulfasalazine
SEM; standard error of the mean
siRNA; small interfering RNA
StRE; stress-response element
tBHQ; *tert*-buthylhydroquione
Tm; tunicamycin
UPS; ubiquitin proteasome system

Abstract

The ubiquitin-proteasome pathway degrades ubiquitinated proteins to remove damaged or misfolded protein and thus plays an important role in the maintenance of many important cellular processes in cells. Because this pathway is also crucial for tumor cell growth and survival, proteasome inhibition by specific inhibitors exhibits potent anti-tumor effects in many cancer cells. xCT, a subunit of the cystine antiporter system x_c^- plays an important role in cellular cysteine and glutathione homeostasis. Several recent reports have revealed that xCT is involved in cancer cell survival, however it was unknown whether xCT affect cytotoxic effect of proteasome inhibitors. In this study, we found that two stress-inducible transcription factors, Nrf2 and ATF4, were upregulated by proteasome inhibition and cooperatively enhance human *xCT* gene expression upon proteasome inhibition. In addition, we demonstrated that the knockdown of xCT by siRNA or pharmacological inhibition of xCT by sulfasalazine (SASP) or (*S*)-4-carboxyphenylglycine (CPG) significantly increased the sensitivity of T24 cells to proteasome inhibition. These results suggest that the simultaneous inhibition of both the proteasome and xCT could have therapeutic benefits in the treatment of bladder tumors.

1. Introduction

1.1 The ubiquitin proteasome system and function.

The ubiquitin proteasome system (UPS) is the major pathway for intracellular protein degradation (1-3) (Fig. 1.1). The proteasome selectively degrades ubiquitinated substrate proteins to eliminate damaged or misfolded proteins and recycles intracellular amino acids. Thus, proteasome activity is required for many important cellular processes such as cell cycle progression, proliferation and apoptosis (1-3).

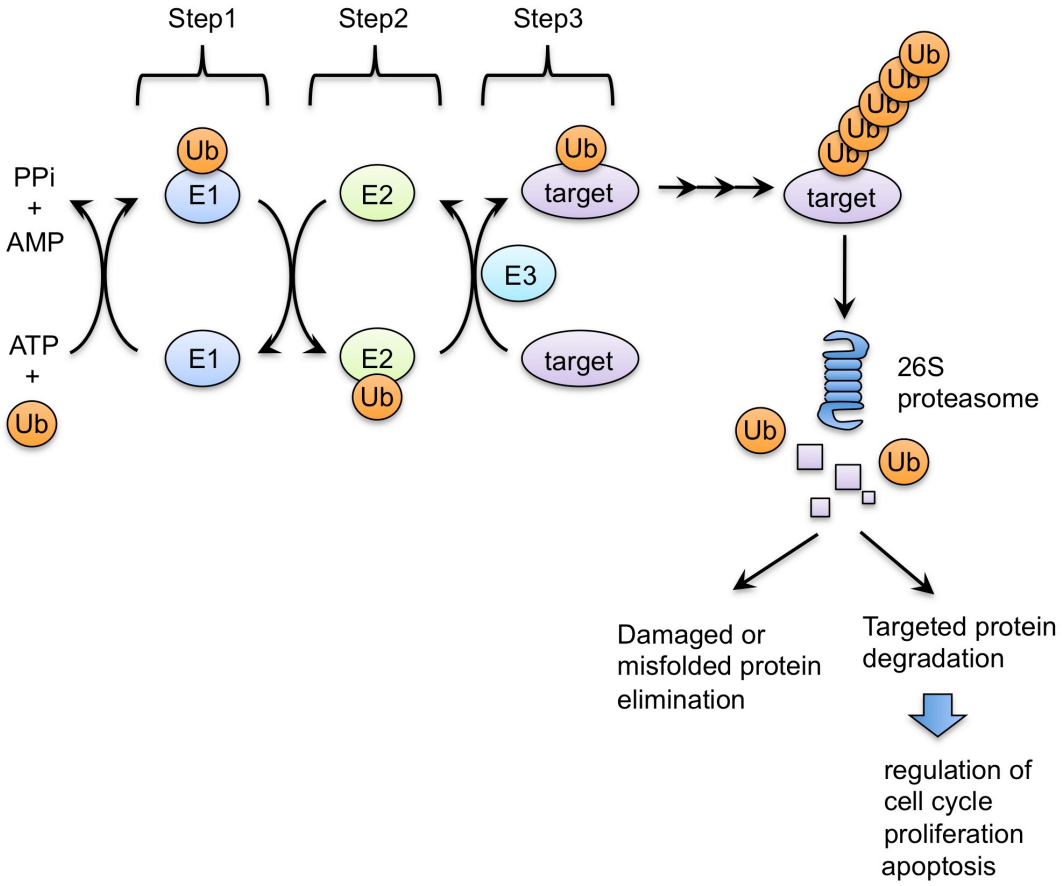

Figure 1.1. The ubiquitin-proteasome system.

1.2 Development of proteasome inhibitors as anti-cancer drugs.

A number of different types of agents have been reported as proteasome inhibitors, such as MG132, bortezomib (BTZ), epoxomicin (EPO) and carfilzomib (CFZ) (4-6) (Fig. 1.2). Because proteasome inhibitors induce cancer cell death via the induction of proteotoxicity, oxidative stress and ER stress, some of these agents are considered anti-cancer drugs (4-6). For example, BTZ (also known as Velcade or PS-341) and CFZ have been approved by Food and Drug Administration (FDA) for the treatment of patients with mantle cell lymphoma (MCL) and multiple myeloma (7-9). However, differential sensitivities to BTZ were observed among cancer cell lines, though these lines were derived from the same tissues (9-14). To increase the efficacy of BTZ, combination therapies using BTZ and other chemotherapeutic agents or therapies have been studied (11, 12, 15). However, it is important to clarify the molecular mechanisms that affect the efficacy of proteasome inhibitors in cancer cells.

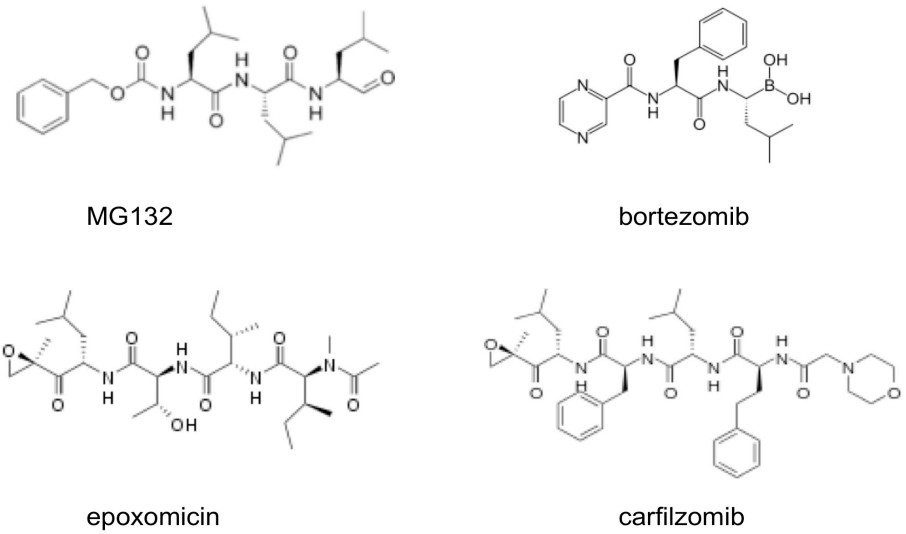

Figure 1.2. Chemical structure of proteasome inhibitors.

1.3 Current bladder cancer treatments.

Bladder cancer is a common worldwide disease, especially in developed countries (16). In the United States, more than 70,000 cases were newly diagnosed in 2012, resulting in approximately 15,000 deaths, most of which occurred as a result of metastatic progression (17). Although approximately 70% of bladder tumors can be cured by surgical removal, approximately 60% to 70% of patients experience local or distant recurrences and almost 20% to 30% of these relapsed tumors progress to higher grades or stages (18). In bladder cancer treatment, *Mycobacterium bovis* bacillus Calmette-Guérin (BCG) administration, radiation and chemotherapy are often beneficial in addition to surgical resection (17-19). In chemotherapy, the recurrent tumors occasionally became more malignant and resistant to the anti-cancer drugs that were initially used. Proteasome inhibitors could be alternative agents for bladder cancer chemotherapy because strong cytotoxic effects were observed in some bladder carcinoma cell lines upon BTZ treatment (10). However, different degrees of resistance to BTZ were also observed among these cell lines (10, 11).

1.4 Function of system x_C^- cystine/glutamate antiporter and cysteine transporter LAT2.

Intracellular cysteine plays an important role in GSH synthesis, which is indispensable for maintaining intracellular redox balance and drug metabolism (20-22). Cell membrane transporters for both cystine and cysteine maintain the level of intracellular cysteine (Fig. 1.3A and B). System x_C^- is a sodium-independent amino acid antiporter, which transports extracellular cystine into cells in exchange for intracellular glutamate at a ratio of 1:1 (23-25) (Fig. 1.3A). It consists of a specific light chain, xCT (also named SLC7A11), and a heavy chain of the 4F2 cell surface antigen 4F2hc (also known as CD98/SLC3A2) (23-25). Not only transporting extracellular cystine into cells, system x_C^- creates a reducing extracellular environment by the cystine/cysteine redox cycle (20, 23-25). On the other hand, cell surface neutral amino acid transporters transport cysteine into the cells (Fig. 1.3B).

xCT is highly expressed in several human cancers, and its expression is associated with malignancy, drug resistance and poor survival in patients (22, 24, 26-28). In addition, a CD44 variant promotes tumor growth by stabilizing the xCT protein (29). Therefore, xCT has been considered a potential therapeutic target and a novel marker for predicting malignancy.

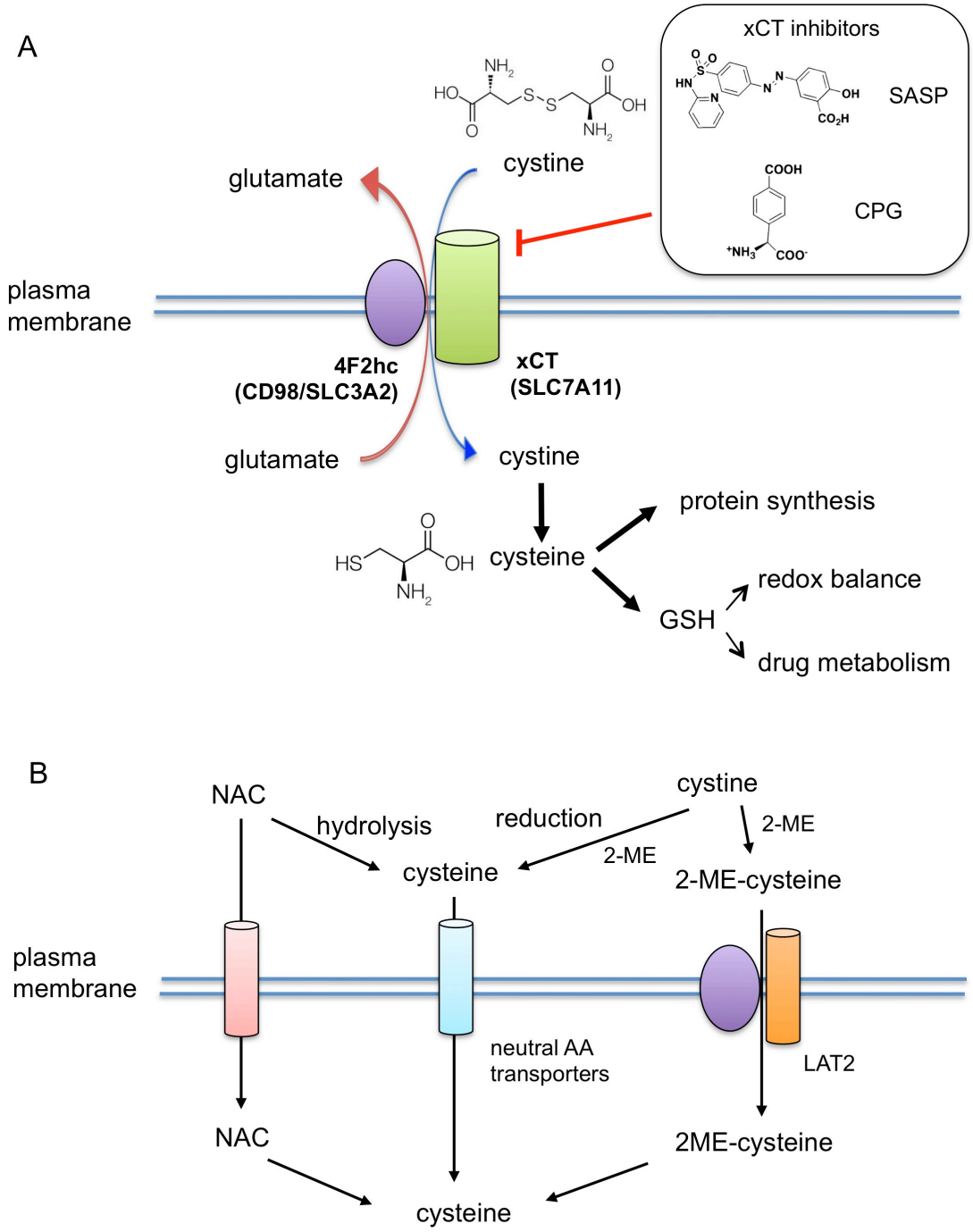

Figure 1.3. (A) The component and function of system x_C^-. (B) Alternative intracellular cysteine supplementation by different amino acid transporters. Cystine in the extracelluar space are transported by system x_C^- or transported by neutral amino acid transporters after reduction to cysteine by reductants such as 2-mercaptoethanol (2-ME). Sulfasalazine (SASP) or (*S*)-4-carboxyphenylglycine (CPG) inhibits the activity of system x_C^-. NAC; *N*-Acetyl-L-cysteine.

1.5 *xCT* gene regulation by Nrf2 pathway.

The expression of xCT is induced by various stimuli, including oxidative stress, amino acid deprivation, bacterial lipopolysaccharides and nitric oxide (30-33). The oxidative stress-responsive transcription factor NF-E2 related factor 2 (Nrf2) mediates xCT induction upon oxidative stress (30, Fig. 1.4). Nrf2 modulates the cytoprotective response and drug metabolism through the induction of its target genes, such as glutamate-L-cysteine ligase catalytic subunit (GCLC) and glutathione-*S*-transferases (GSTs) (34, 35). In unstressed condition, Nrf2 is constitutively degraded through the UPS and repressed. In response to oxidative stress, Nrf2 activates target gene expression in an antioxidant response element (ARE, also referred as electrophile response element (EpRE))-dependent manner. The consensus sequence of ARE is GCnnnGTCAC/T (n=any base).

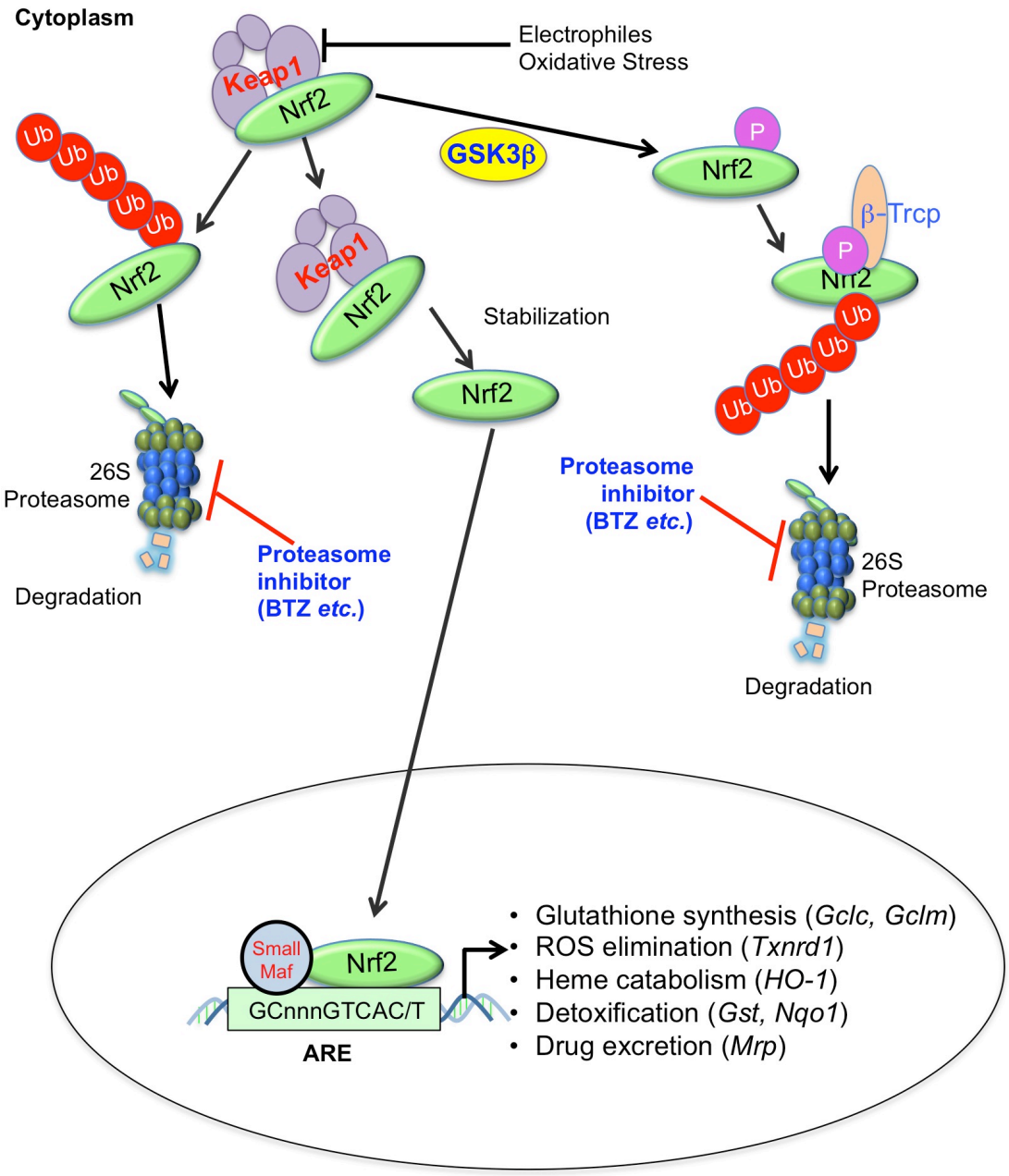

Figure 1.4. The Nrf2 activation pathway and its target genes. Under unstressed conditions, Nrf2 is degraded through the UPS. Electrophile sensor protein Keap1 acts as the substrate adaptor protein for culllin3 ubiquitin E3 ligase. Upon oxidative stress, Keap1 is inactivated. Then, Nrf2 degradation is suppressed and newly synthesized Nrf2 translocates to the nucleus. In the nucleus, Nrf2 heterodimerizes with small Maf (sMaf) and binds to ARE, and subsequently activates the expression of these genes. On the other hand, GSK3β phosphorylates Nrf2, promoting the β-TrCP-mediated ubiquitination and subsequent degradation of Nrf2 in the nucleus. Activated Akt phosphorylates GSK3β and inhibits the activity of this kinase. Therefore, the activation of the PI3K/Akt pathway enhances Nrf2 accumulation through the inhibition of β-TrCP-dependent degradation.

1.6 *xCT* gene regulation by ATF4 pathway.

Activating transcription factor 4 (ATF4) mediates xCT expression during amino acid deprivation and oxidative stress (31, 36, Fig. 1.5). This protein is a basic leucine zipper (bZip) transcription factor that is activated by multiple stress signals including amino acid deprivation, heme deficiency and endoplasmic reticulum (ER) stress (37, 38, 39). In stress conditions, ATF4 is selectively translated by the phosphorylation of eukaryotic initiation factor 2α (eIF2α), and it upregulates its target genes by binding to the amino acid response elements (AAREs) in their regulatory regions. The consensus sequence of AARE is TGATGnAAn (n=any base). In the mouse *xCT* gene promoter, one ARE and two AAREs mediate oxidative stress- and amino acid deprivation-induced *xCT* gene expression, respectively (30, 31). However, the regulatory mechanism of human the *xCT* gene remains poorly understood. Interestingly, both Nrf2 and ATF4 are activated by proteasome inhibition (32).

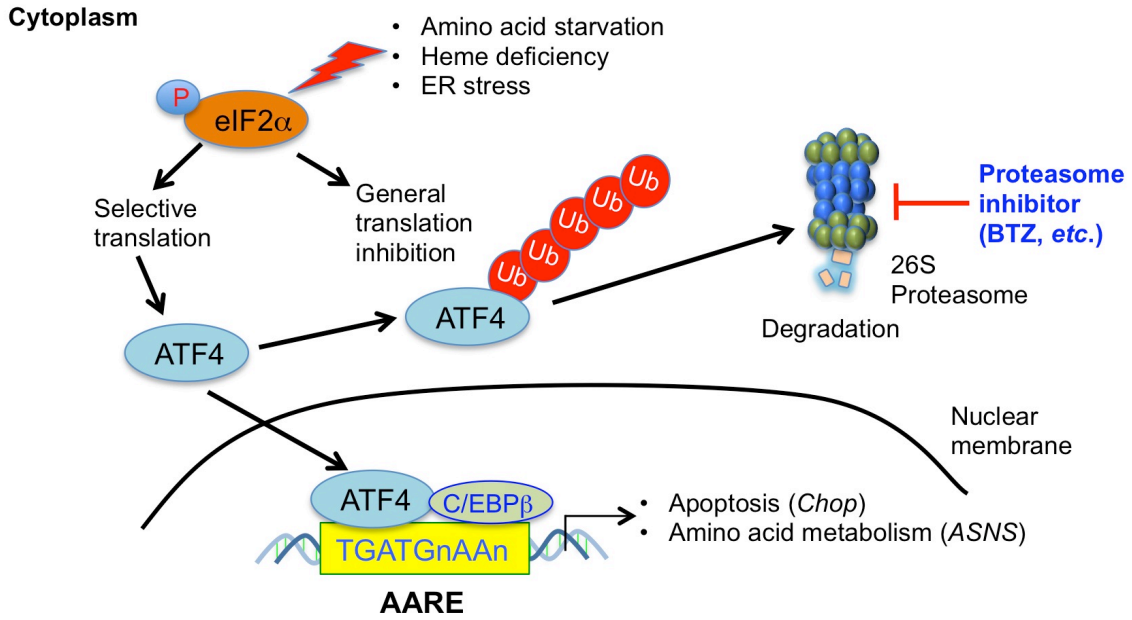

Figure 1.5. The ATF4 activation pathway and its target genes. eIF2α is phosphorylated by various stresses including amino acid starvation, heme deficiency and ER stress. While phosphorylation of

eIF2α causes the inhibition of general translation, it selectively enhances the translation of cytoprotective proteins such as ATF4. ATF4 is also degraded through UPS.

1.7 The aim of this study.

The bladder carcinoma cell line T24 exhibits relatively high resistance to BTZ, but the underlying mechanism of T24 resistance to BTZ was unknown. In previous study, we found that *xCT* gene expression is highly inducible in T24 cells by BTZ treatment. In addition, other researchers have reported the relationship between cancer cell survival and xCT expression (22, 24-28). The aim of this study was to elucidate the precise regulatory mechanism of *xCT* gene induction by proteasome inhibitors and the role of the xCT induction in T24 resistance to proteasome inhibitors. This study also aimed to investigate the benefit of simultaneous inhibition of both the proteasome and xCT pathway in the bladder cancer treatment.

2 Materials and Methods

2.1 Materials.

BTZ was obtained from Cell Signaling Technology (Danvers, MA, USA). EPO and MG132 were obtained from Peptide Institute (Osaka, Japan). CFZ was obtained from Selleck Chemicals (Houston, TX, USA). CPG was obtained from Tocris Bioscience (Bristol, UK). Dulbecco's modified Eagle medium (DMEM), NAC, SASP and tunicamycin (Tm) were obtained from Sigma-Aldrich (St. Louis, MO, USA). *tert*-buthylhydroquione (tBHQ) was obtained from Kanto Chemical (Tokyo, Japan). Dimethylsulfoxide (DMSO) and 2-ME were obtained from Wako Pure Chemical (Osaka, Japan). Bovine serum albumin (BSA) was purchased from Nakalai Tesque (Kyoto, Japan). Anti-Nrf2 antibody (sc-722 or sc-13032), anti-ATF4 antibody (sc-200) and anti-Lamin B antibody (sc-6217) as well as normal rabbit IgG were purchased from Santa Cruz Biotechnology (Dallas, TX, USA). Anti-xCT antibody (ab37185) was obtained from Abcam (Cambridge, MA, USA). Anti-eIF2α and anti-phospho-eIF2α (Ser51) antibodies were purchased from Cell Signaling Technology (Beverly, MA, USA).

2.2 Cell culture.

The human bladder cancer cell line T24, the human cervix carcinoma cell line HeLa, human astrocytoma cell line U373MG, human glioblastoma cell line T98G and human embryonic kidney 293T cell line were maintained in DMEM containing 10% fetal bovine serum (Gibco, Grand Island,

NY, USA) with 100 U/mL penicillin and 100 μg/mL streptomycin (Gibco). The cells were cultured at 37 °C with 5% CO_2 and saturated humidity.

2.3 RNA preparation and RT-qPCR.

Total RNAs from T24 and HeLa cells were isolated using TRIzol reagent (Life technologies, Carlsbad, CA, USA) according to the manufacturer's protocol. cDNAs were synthesized using the PrimeScript II 1st strand cDNA Synthesis kit (Takara Bio, Otsu, Japan). The quantitative RT-PCR (RT-qPCR) analyses were performed using SYBR Premix Ex Taq II (Takara Bio) and the CFX Real-Time PCR Detection System (Bio-Rad, Hercules, CA, USA). The primers used for RT-qPCR were designed as below (Table 1) Cyclophilin A (CypA) was used as an internal control.

Table 1 The primers used for RT-qPCR.

Primers	Sequence
human xCT forward	5’-CCA TGA ACG GTG GTG TGT T-3’
human xCT reverse	5’-GAC CCT CTC GAG ACG CAA C-3’
human GCLC forward	5’-TTG ACG ATA GAT AAA GAG ATC TAC GAA-3’
human GCLC reverse	5’-TCT CTA ATA AAG AGA TGA GCA ACA TGC-3’
human GCLM forward	5’-TGG GCA CAG GTA AAA CCA A-3’
human GCLM reverse	5’-CAG TCA AAT CTG GTG GCA TC-3’
human survivin/BIRC5 forward	5’-AGA ACT GGC CCT TCT TGG A-3’
human survivin/BIRC6 reverse	5’-CAA GTC TGG CTC GTT CTC AGT-3’
human Hsp72/HSPA2 forward	5’-GCG ACA AAT CAG AGA ATG TGC-3’
human Hsp72/HSPA3 reverse	5’-GTG GTG TTC CTC TTG ATG AGT G-3’
human PSMB5 forward	5’-GAG TCT CAG TGA TGG TCT GAG C-3’
human PSMB6 reverse	5’-GAC TCC ATG GCG GAA CTT GA-3’
human Cyclophilin A forward	5’-ATG CTG GAC CCA ACA CAA AT-3’
human Cyclophilin A reverse	5’-TCT TTC ACT TTG CCA AAC ACC-3’

2.4 Immunoblot analysis.

Whole cell lysates were prepared by dissolving the cell pellets directly into sample buffer (62.5 mM Tris-HCl (pH 6.8), 2% SDS and 10% glycerol) and then sonicated to shear the DNA. Protein concentrations were quantified using a BCA protein assay kit (Thermo Fisher Scientific, Waltham, MA, USA) according to the manufacturer’s protocol. After protein quantification, 2-ME (final 1%) and bromophenol blue (final 0.01%) were added to each sample, and the samples were incubated at 100 °C for 5 min. or at RT for 30 min. (for xCT detection). Fifteen micrograms of protein per each lane was separated by 6 to 10% SDS-PAGE and then transferred onto PVDF membranes (Millipore, Billerica MA, USA). The membranes were blocked with 1% skim milk-PBS with 0.1% Tween-20 (PBST) or 1% BSA-PBST (for xCT and eIF2α blots) and then blotted with anti-Nrf2, anti-ATF4, anti-xCT, anti-eIF2α,

anti-phospho-eIF2α or anti-Lamin B antibodies. After washing with PBST, the membranes were incubated with horseradish peroxidase-conjugated secondary antibodies and then visualized using ImmunoStar chemiluminescent reagent (Wako Pure Chemical).

2.5 siRNA (small interfering RNA) transfection.

T24 cells and HeLa cells were transfected with siRNAs targetting human ATF4, Nrf2 or xCT or scramble siRNA using Lipofectamine RNAiMAX (Life Technologies). The siRNAs were synthesized as below (Table. 2) and scramble siRNA was purchased from Qiagen (Hilden, Germany). Four hours after transfection, the medium was replaced with fresh medium. After 20 h of incubation, the transfected cells were treated with chemicals for the indicated times and subjected to immunoblot or RT-qPCR analysis.

Table 2 The sequence of siRNAs used in knockdown experiments.

Primers	**Sequence**
anti-human ATF4 sense	5'-GCC UAG GUC UCU UAG AUG ATT-3'
anti-human ATF4 antisense	5'-UCA UCU AAG AGA CCU AGG CTT-3'
anti-human Nrf2 sense	5'-GUA AGA AGC CAG AUG UUA ATT-3'
anti-human Nrf2 antisense	5'-UUA ACA UCU GGC UUC UUA CTT-3'
anti-human xCT sense	5'-AGA GAC AUG CCC ACG CUG CTT-3'
anti-human xCT antisense	5'-GCA GCG UGG GCA UGU CUC UTT-3'

2.6 Chromatin immunoprecipitation (ChIP) analysis.

ChIP analysis was performed as previously described with few modifications (40, Fig. 2.1). In brief,

T24 cells were incubated with 100 nM BTZ for 6 h and then fixed with 1% formaldehyde for 10 min at 37 °C. After fixation, the cells were collected and sonicated to prepare chromatin suspensions of DNA approximately 300 bp in length. Subsequently, the lysates were incubated with anti-Nrf2 (sc-13032) or anti-ATF4 (sc-200) antibodies O/N at 4 °C. Normal rabbit IgG (sc-2027) was used as a negative control. After antigen-antibody reaction, immunocomplexes were captured with Protein G-Sepharose Fast Flow beads (GE Healthcare, Littel Chalfont, UK), and coimmunoprecipitated DNA fragments were purified. The relative amounts of immunoprecipitated DNA fragments were evaluated by qPCR using following primer pairs: human *xCT* gene promoter region: forward 5'-TTG AGC AAC AAG CTC CTC CT-3' and reverse 5'-CAA ACC AGC TCA GCT TCC TC-3'; human *xCT* gene intron 1 region: forward 5'-ATT GCA GGG AGT GTG CTC TT-3' and reverse 5'-TCA GAT TTT GCT TTG CTT GC-3'; human *xCT* gene intron 2 region: forward 5'-AGA CAC TTC TGT GCC TCA CAA C-3' and reverse 5'-CTT CCC ACA AAG TCG AAG GA-3'.

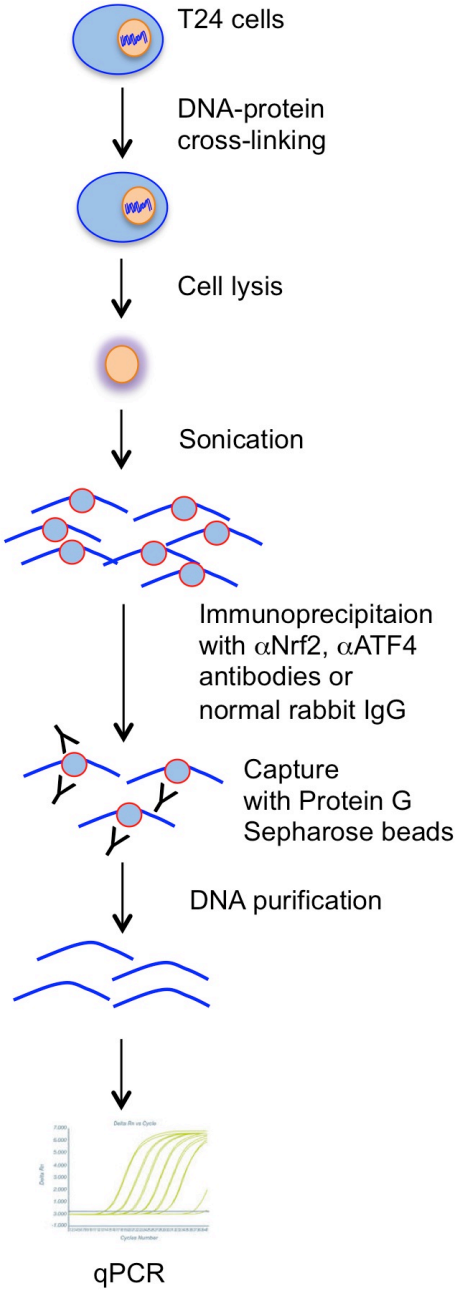

Figure 2.1. Schematic illustration of ChIP assay.

2.7 Plasmid construction.

To construct the human *xCT* gene promoter-luciferase reporter plasmid (pxCT pro WT-Luc), an approximately 0.7 kb DNA fragment of the human *xCT* gene promoter was amplified by PCR using the following primers (forward 5'-GGC TAG CTC TGG AGT CAT GGT GAA TTT TG-3'; reverse 5'-GGG AGA TCT ACA AAC CAG CTC AGC TTC CT-3'). The amplified DNA fragment was digested with NheI and BglII and then subcloned into the NheI/BglII sites of the pGL3 basic vector. The ARE mutant reporter plasmid (pxCT pro-mt1-Luc) was generated by site-directed mutagenesis using the following primer pair (forward 5'-AAA GAG CTG AGC ACT GCT GGA GGC TTC TCA TGT GG-3'; reverse 5'-CCA CAT GAG AAG CCT CCA GCA GTG CTC AGC TCT TT-3'). The construct with mutations in both AAREs (pxCT pro-mt2-Luc) was generated by site-directed mutagenesis using the following primer pairs (forward 5'-AGG CTT CTC ATG TGG CGG GTG CAA ACC TGG AG-3'; reverse 5'-CTC CAG GTT TGC ACC CGC CAC ATG AGA AGC CT-3'), and (forward 5'-GCA AAC CTG GAG AAT TTG CAC CCT CAT TTA GCT GTA GTA AG-3'; reverse 5'-CTT ACT ACA GCT AAA TGA GGG TGC AAA TTC TCC AGG TTT GC-3'). To construct pSV-Luc-xCT int WT, a portion of the second intron of the human *xCT* gene was PCR-amplified using the following primers (forward 5'-GCG GAT CCA TTC CTG CTT GTC TTG GTT T-3'; reverse 5'-GCG TCG ACT CAG ACT GTG CAC ATC ACA TTT-3') and digested with BamHI and SalI. It was then subcloned into the BamHI/SalI sites of the pGL3 promoter vector. pSV-Luc-xCT int mt was constructed by site-directed mutagenesis using the following primer pair (forward 5'- CAC ACT GAA

TAG TGC TAA GCC CCT CTG AAT AGC AAA TTT CC-3'; reverse 5'- GGA AAT TTG CTA TTC AGA GGG GCT TAG CAC TAT TCA GTG TG-3'). The expression plasmid pcDNA3-hNrf2 was prepared as previously described (40). pcDNA3-hATF4 was produced by subcloning PCR-amplified human ATF4 cDNA into the BamHI/EcoRI sites of the pcDNA3 vector as described elsewhere. To construct GST-hATF4 full-length expression vector (pGEX-hATF4), full-length human ATF4 cDNA was PCR amplified by using primers (5'-CGG ATC CCG CAA CAT GAC CGA AAT GAG C -3' and 5'-GGA ATT CTA TCC TCA ACT AGG GGA CCC T-3'). The PCR amplified cDNA fragment was digested with BamHI and EcoRI, and then subcloned into BamHI/EcoRI sites of pGEX-6P-2 vector (GE Healthcare). To construct pGEX-hATF4 (1-143), pGEX-hATF4 (144-269) and pGEX-hATF4 (270-351), corresponding human ATF4 cDNA fragments were PCR amplified by using following primer sets containing restriction enzyme site at its 5' end: 5'-CGG ATC CCG CAA CAT GAC CGA AAT GAG C-3' and 5'-GCG AAT TCG ATG GCC AAT TGG GTT CAC CGT-3' for hATF4 (1-143), 5'-CGG ATC CCT CCC AGA AAG TTT AAC AAA ACC C-3' and 5'-GGG CTC GAG TAC CAT CTT CTC TCC AGG AGG ATC-3' for hATF4 (144-269), 5'-GCG AAT TCT AGC AGC AAA AGT AAA GGG TGA GA-3' and 5'-GGG CTC GAG CAC ATT GAC GCT CCT GAC TAT C-3' for hATF4 (270-351). The PCR amplified human ATF4 cDNA fragments were digested with restriction enzymes and subcloned into pGEX-6P-2 vector. To construct of pGEX-hNrf2, human Nrf2 cDNA fragment was PCR amplified by using following primers (5'-CGG GAT CCC CAT GAT GGA CTT GGA GCT GCC-3' and 5'-CCG CTC GAG CCT AAA TCT AGT TTT TCT AAT C-3'). Amplified Nrf2 cDNA

fragment was digested with BamHI and XhoI, and subcloned into BamHI/XhoI sites of pGEX-5X-1 vector (GE Healthcare). To construct pGEX-hNrf2 (1-209), pGEX-hNrf2 (210-419) and pGEX-hNrf2 (420-605), corresponding human Nrf2 cDNA fragments were PCR amplified by using following primer sets: 5'-GCG GAT CCC TCA TCA TGA TGG ACT TGG AGC-3' and 5'-GGG CTC GAG CTC AAC CAG CTT GTC ATT TTC AAT ATT A-3', 5'-GCG GAT CCA CTA CCA TGG TTC CAA GTC CAG AA-3' and 5'-GGG CTC GAG ATC ATG CAC GTG AGT GCT CTG C-3', 5'-GCG GAT CCA CCA TGG CCC AAT GTG AGA ACA CAC CA-3' and 5'-GGG CTC GAG GTC AAA TCC TCC TAA ATC TAG TTT-3', respectively. The PCR amplified Nrf2 cDNA fragments were subcloned into pGEX-6P-2 vector.

2.8 Reporter assay.

The day before transfection, HeLa cells were seeded on 24-well plates at a density of 5.0 x 10^4 cells/well (Fig. 2.2). The next day, the cells were cotransfected with the luciferase reporter plasmids and the effector plasmids using FuGENE HD Transfection Reagent (Promega, Madison, WI, USA). pRL-TK was used as an internal control. Four hours after transfection, the media was replaced with fresh media, and the cells were incubated for an additional 20 h. T24 cells were transfected as indicated above except that Lipofectamine 2000 (Life Technologies) was used as the transfection reagent. Twenty-four hours after transfection, the cells were incubated for another 6 h in the presence or absence of 100 nM BTZ. Luciferase activity was measured using Dual luciferase assay kits (Promega),

according to the manufacturer's recommended protocol.

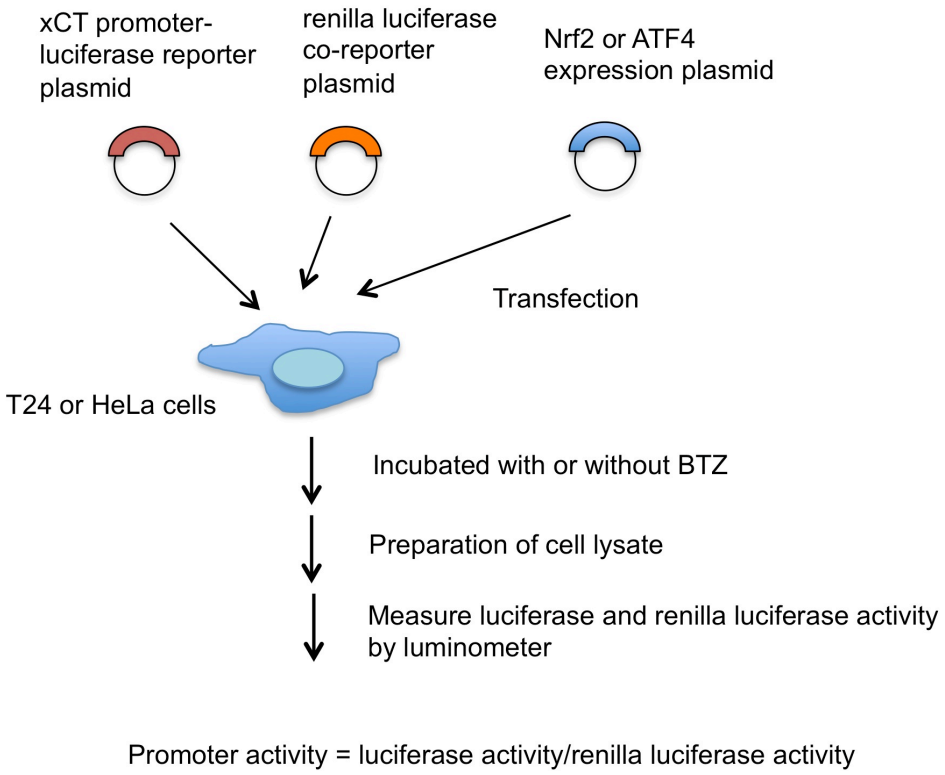

Figure 2.2. Schematic illustration of reporter assay.

2.9 Glutathione S-transferase (GST) pull-down assay.

GST pull-down assay was performed by a conventional method (Fig. 2.3). Briefly, *Escherichia coli* JM 109 carrying GST or GST-fusion protein expression vectors were incubated at 37°C for 90 min. in the presence of 0.5 mM IPTG. The bacterial cell pellet was suspended in bacteria lysis buffer (40 mM Tris-HCl (pH 7.5)-5 mM EDTA-0.5% Trion X-100 with 1x protease inhibitor cocktail (EDTA-free) (Roche, Basel, Switzerland)). After brief sonication, bacterial lysate was cleared by centrifugation and the supernatant was then incubated with glutathione sepharose 4B beads slurry (GE Healthcare) for 1 h

at 4°C. The GST fusion protein bound beads were divided into two and one was subjected to SDS-PAGE and stained with Bio Safe Coomassie stain (BIO-RAD), and the other was used for GST pull-down experiment. The remaining GST fusion protein bound beads were incubated with 293T whole cell extract expressing FLAGx3-hATF4 or FLAGx3-hNrf2 at 4°C for 4 h and washed twice with washing buffer (50 mM Tris-HCl (pH 8), 150 mM NaCl, 1 mM EDTA, 1% Triton X-100, 1.5 mM $MgCl_2$-10% glycerol). The pull-downed sample was separated with SDS-PAGE and subjected to immunoblot analysis. To prepare 293T whole cell extract expressing FLAGx3-hATF4 or FLAGx3-hNrf2, 293T cells were transiently transfected with either FLAGx3-hATF4 or FLAGx3-hNrf2 expression plasmids. After 24 h transfection, the cells were treated with 5 μM MG132 for 6 h and then the cell pellet was collected. The cell pellet was dissolved in cell lysis buffer (50 mM Tris-HCl (pH 8), 300 mM NaCl, 1 mM EDTA, 1% Triton X-100, 1.5 mM $MgCl_2$, 10% glycerol with 1x EDTA free protease inhibitor cocktail and 1x PhosSTOP (Roche)), and incubated 30 min on ice. After centrifugation, the supernatant was diluted with equal volume of dilution buffer (50 mM Tris-HCl (pH 8)-1 mM EDTA-1% Triton X-100-1.5 mM $MgCl_2$-10% glycerol with 1x EDTA free protease inhibitor cocktail and 1x PhosSTOP) and kept as whole cell extract.

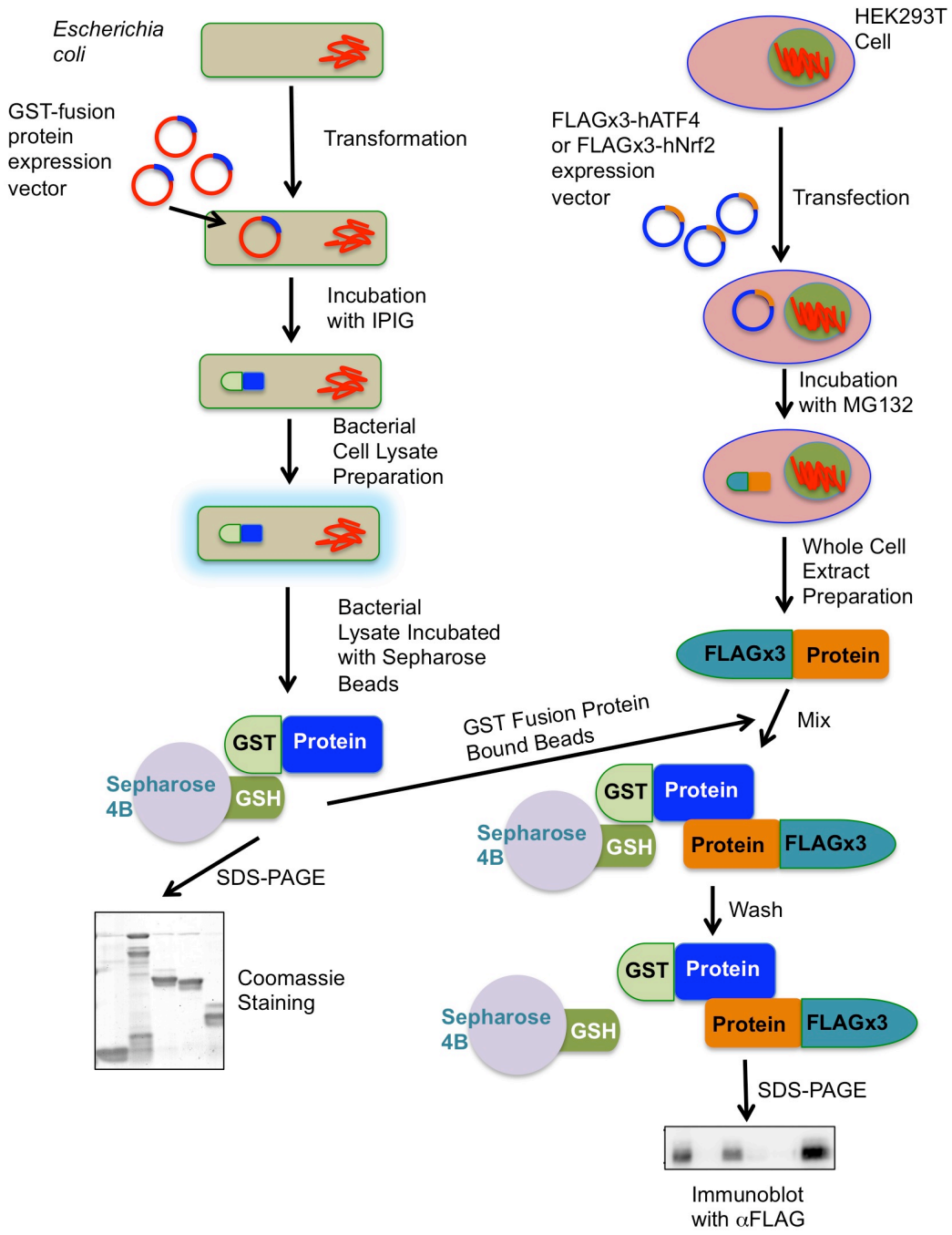

Figure 2.3. General schematic illustration of GST pull-down assay.

2.10 Cell viability analysis.

T24 cells were plated on 6-well plates at a density of 3.0 x 10^5 cells/well (Fig. 2.4). The next day, the cells were transfected with control or xCT siRNA as described above. Twenty-four hours after

transfection, the transfected cells were re-seeded on 96-well plates at a density of 3.0 x 10^4 cells/well and incubated overnight. The following day, 5 to 100 nM BTZ or 10 nM EPO were added to the transfected cells and incubated for an additional 48 h. For SASP or CPG treatment experiments, T24 cells were seeded on 96-well plates at a density of 5.0 x 10^4 cells/well. After 24 h, the culture media were replaced with media containing 0.3 mM SASP or 0.2 mM CPG for 6 h or 30 min, and then the cells were administrated with increasing doses of proteasome inhibitors for an additional 48 h. In some experiments, 66 μM 2-ME was added. Cell viability was evaluated using the Cell Counting Kit-8 (CCK-8) (Dojindo Molecular Technologies, Kumamoto, Japan) according to the manufacturer's recommended protocol.

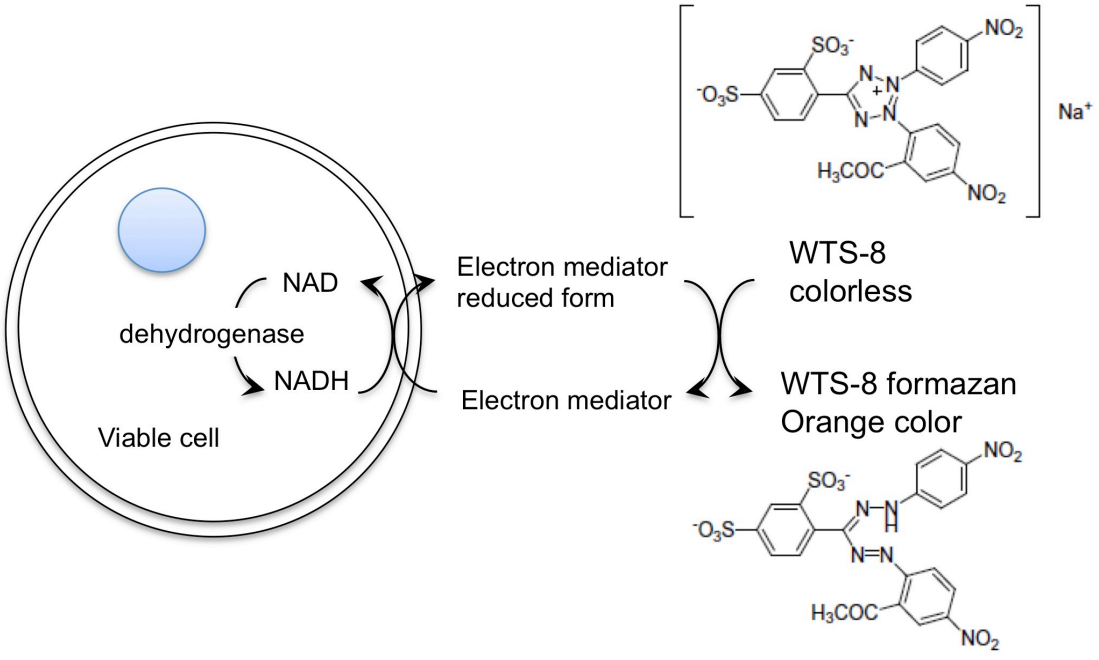

Figure 2.4. Principle of the cell viability detection with CCK-8.

2.11 Intracellular cysteine and GSH measurements.

T24 cells were plated on 6-well plates at a density of 3.0 x 10^5 cells/well and incubated overnight. The following day, the cells were transfected with either control or anti-xCT siRNA as described above. Twenty-four hours after transfection, the cells were incubated in the presence or absence of 20 nM BTZ for 18 h. For SASP treatment experiments, T24 cells were seeded on 6-well plates at a density of 6.0 x 10^5 cells/well. After 24 h incubation, the cells were pretreated with 0.3 mM SASP for 6 h, and then treated with 20 nM BTZ for additional 24 h. Intracellular cysteine and GSH levels were measured as previously described by using monobromobimane (mBBr) and HPLC (30, Fig. 2.5).

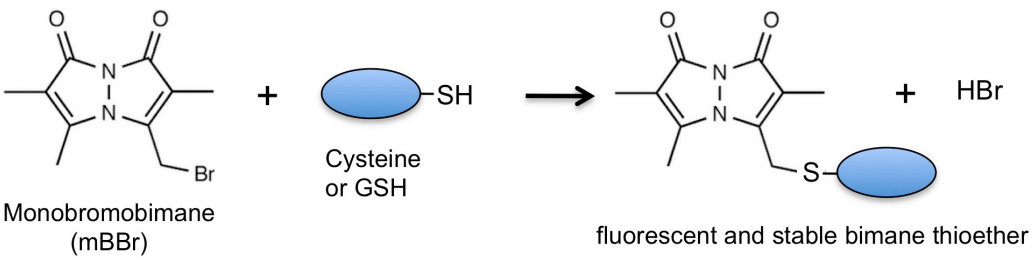

Figure 2.5. Reaction of mBBr with thiol (GSH and cysteine). Nonfluorescent monobromobimane alkylates thiol groups, displacing the bromine and adding the bimane moiety to the thiol of cysteine or GSH.

2.12 Statistical analysis.

The data are presented as the means±SEM. The Student's *t*-test or one-way analysis of variance (ANOVA) with the Bonferroni *post-hoc* test were used to determine significant differences between means. $p<0.05$ was considered significant.

3 Results

3.1 Proteasome inhibitors induce xCT expression in T24 cells.

In a preliminary study, we found that *xCT* mRNA is highly induced in T24 human bladder carcinoma cells by BTZ. To investigate the expression profile of xCT by proteasome inhibitors in T24 cells, we first analyzed *xCT* induction by proteasome inhibitors by RT-qPCR. RT-qPCR analysis revealed that *xCT* mRNA expression was strongly upregulated 9.8-, 13.2- and 15.9-fold by 20, 50 and 100 nM BTZ, respectively, and significantly upregulated from 6 to 24 h (Fig. 3.1A and C). In accordance with these results, marked xCT protein induction was observed in BTZ-treated T24 cells in a dose- and time-dependent manner (Fig. 3.1D and E). Different types of proteasome inhibitors, EPO and MG132, also increased *xCT* mRNA and protein levels in T24 cells (Fig. 3.1B, D, F, G and H). These results indicate that xCT expression is strongly enhanced by proteasome inhibition in T24 cells.

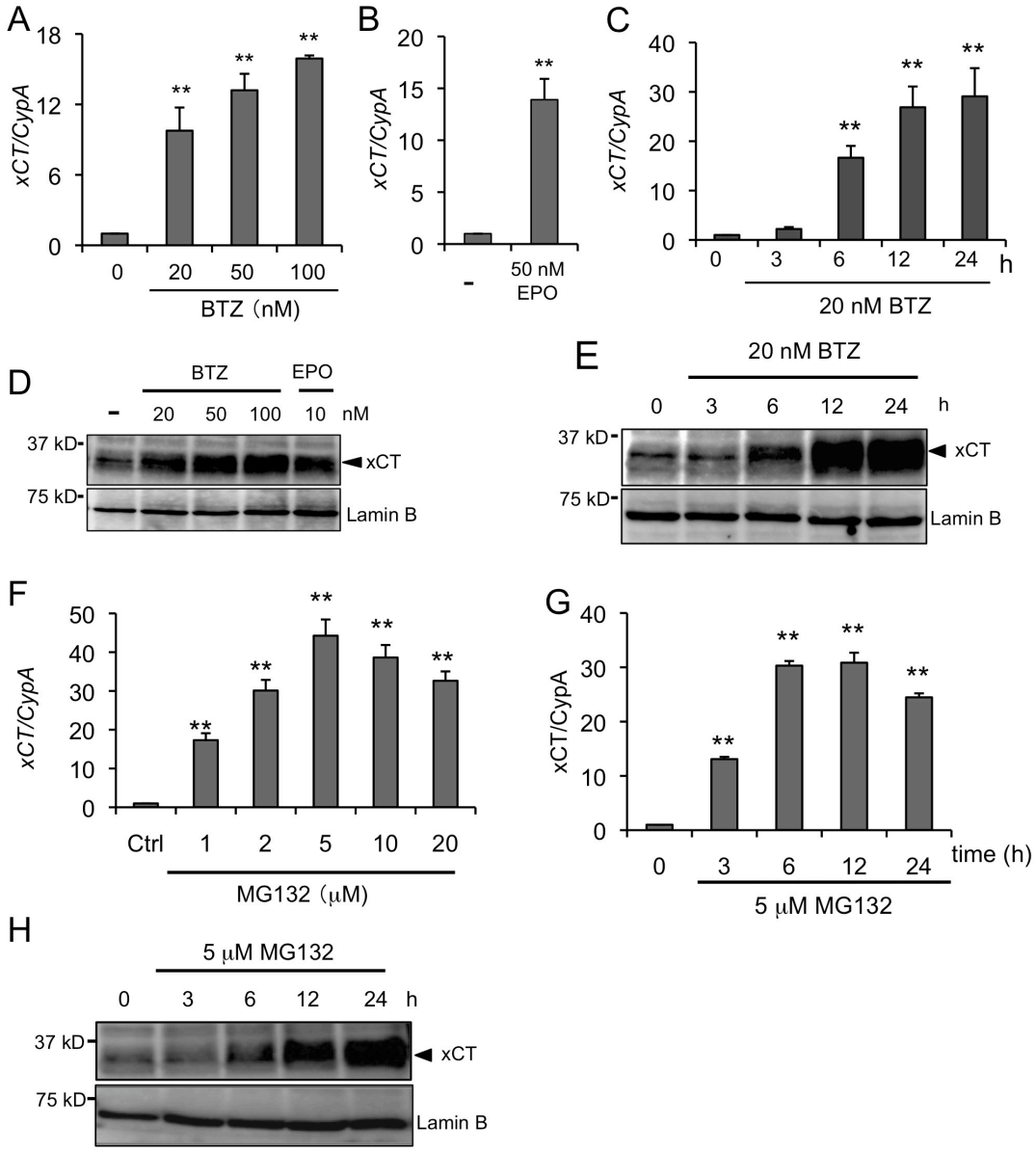

Figure 3.1. Proteasome inhibitors induce xCT in T24 cells. (A), (B) T24 cells were treated with 20 to 100 nM BTZ or 50 nM epoxomicin EPO for 6 h, and then *xCT* mRNA expression was evaluated by RT-qPCR and normalized with CypA expression levels. The data represent means±SEM from three independent experiments. Differences between groups were assessed with one-way ANOVA/Bonferroni *post-hoc* test (A) or Student's *t*-test (B). $^{**}p<0.01$. (C) T24 cells were treated with 20 nM BTZ for 3 to 24 h. *xCT* mRNA expression was evaluated by RT-qPCR. (D) T24 cells were exposed to different amounts of BTZ or 10 nM EPO, as indicated in the figure for 6 h, and then whole cell lysates were subjected to immunoblot analysis. (E) T24 cells were treated with 20 nM BTZ for 3 to 24 h. xCT protein expression was evaluated by immunoblot analysis. Lamin B was used as the loading control. The cells were treated with 1 to 20 μM MG132 for 6 h (F), or with 5 μM MG132 for 3 to 24 h (G), (H) and then subjected to RT-qPCR or immunoblot analysis (F), (G), (H).

3.2 A proteasome inhibitor induces xCT expression in a Nrf2- and ATF4-dependent manner.

Nrf2 and ATF4 modulate *xCT* gene expression in murine cells (30, 31, 36). To investigate the roles of Nrf2 and ATF4 in proteasome inhibitor-induced xCT expression, we analyzed Nrf2 and ATF4 expression in T24 cells. All examined proteasome inhibitors strongly induced both Nrf2 and ATF4 expression in T24 cells, although Nrf2 induction was decreased at high EPO concentration (Fig. 3.2A). Both Nrf2 and ATF4 mRNA and protein were upregulated in time-dependent manners (Fig. 3.2B and C). But, the induction of Nrf2 and ATF4 proteins by BTZ peaked earlier than each mRNA induction suggesting that Nrf2 and ATF4 induction by BTZ might be mainly due to protein stabilization (Fig. 3.2C). Consistent with this hypothesis, eIF2α phosphorylation, which enhances selective translation of ATF4, was not increased by BTZ treatment (Fig. 3.2B). To evaluate the requirement for Nrf2 and ATF4 in BTZ-inducible xCT expression, we next knocked down Nrf2 and/or ATF4 using siRNAs. Nrf2 and ATF4 protein levels after siRNA transfection were detected by immunoblot analysis (Fig. 3.2E). As shown in Fig. 3.2D, Nrf2 and ATF4 knockdown attenuated *xCT* mRNA induction by 20 or 100 nM BTZ treatment, and the simultaneous knockdown of both Nrf2 and ATF4 more effectively decreased *xCT* mRNA expression compared to the single knockdowns. In accordance with the RT-qPCR results, BTZ-induced xCT protein expression was diminished in Nrf2 and ATF4 knockdown cells and further decreased in Nrf2/ATF4 double knockdown cells (Fig. 3.2F). To address the individual effects of Nrf2 and ATF4 activation, T24 cells were treated with Nrf2- or ATF4-specific inducers. Treatment with the Nrf2-specific inducer tBHQ activated Nrf2 and xCT expression in T24 cells (Fig. 3.2G and I, lane 2). Similarly, the ATF4-specific inducer Tm also induced xCT expression (Fig. 3.2G and J, lane 2).

Simultaneous tBHQ and Tm treatment additively enhanced xCT expression (Fig. 3.2H to J). These results suggest that Nrf2 and ATF4, induced by proteasome inhibition, coordinately modulate *xCT* gene expression in T24 cells.

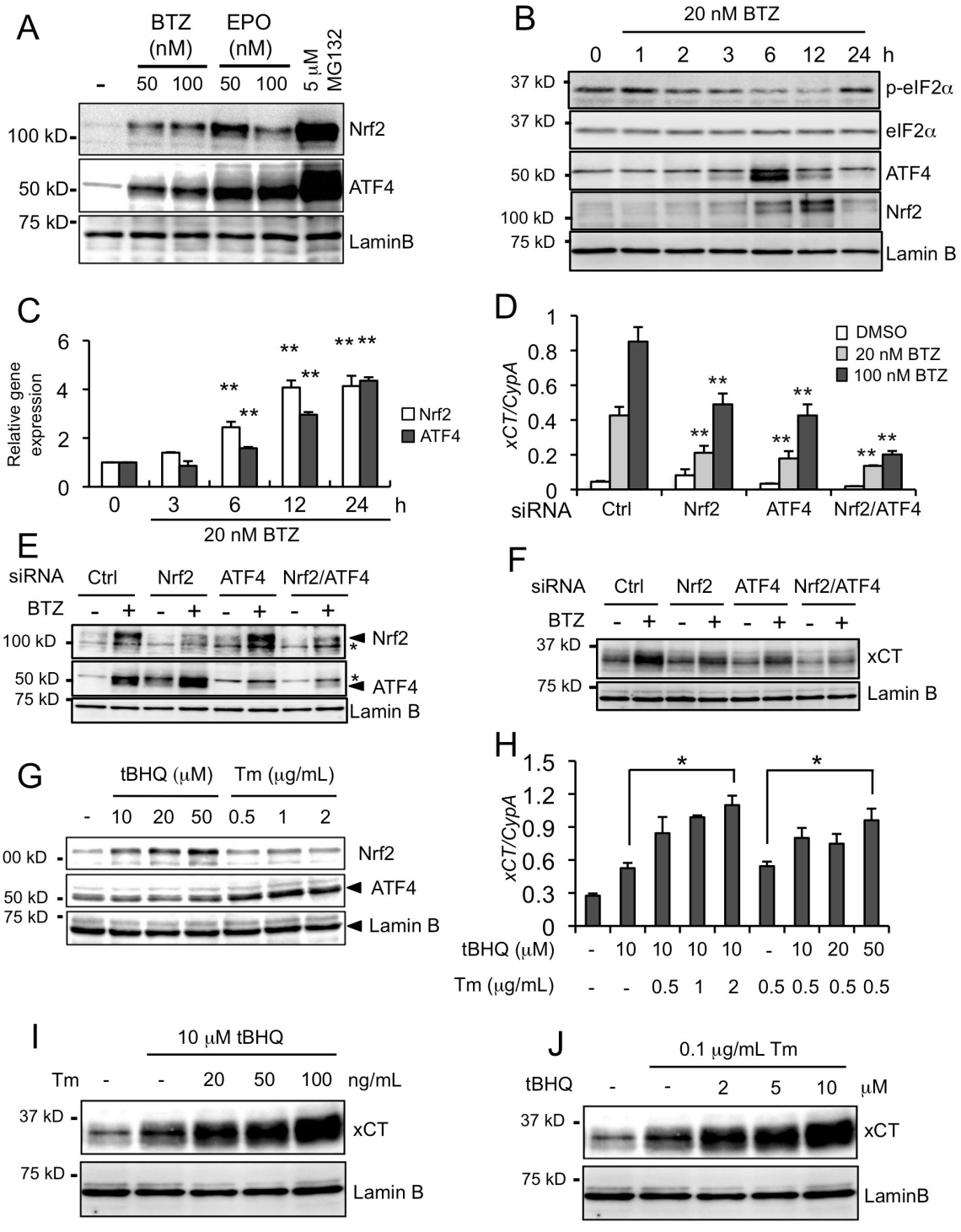
A
BTZ (nM)
EPO (nM)
5 μM MG132
- 50 100 50 100
100 kD
50 kD
75 kD
Nrf2
ATF4
LaminB
B
20 nM BTZ
0 1 2 3 6 12 24 h
37 kD
37 kD
50 kD
100 kD
75 kD
p-eIF2α
eIF2α
ATF4
Nrf2
Lamin B
C
Relative gene expression
Nrf2
ATF4
0 3 6 12 24 h
20 nM BTZ
D
xCT/CypA
DMSO
20 nM BTZ
100 nM BTZ
siRNA Ctrl Nrf2 ATF4 Nrf2/ATF4
E
siRNA Ctrl Nrf2 ATF4 Nrf2/ATF4
BTZ - + - + - + - +
100 kD
50 kD
75 kD
Nrf2
ATF4
Lamin B
F
siRNA Ctrl Nrf2 ATF4 Nrf2/ATF4
BTZ - + - + - + - +
37 kD
75 kD
xCT
Lamin B
G
tBHQ (μM)
Tm (μg/mL)
- 10 20 50 0.5 1 2
100 kD
50 kD
75 kD
Nrf2
ATF4
Lamin B
H
xCT/CypA
tBHQ (μM) - 10 10 10 10 - 10 20 50
Tm (μg/mL) - - 0.5 1 2 0.5 0.5 0.5 0.5
I
10 μM tBHQ
Tm - - 20 50 100 ng/mL
37 kD
75 kD
xCT
Lamin B
J
0.1 μg/mL Tm
tBHQ - - 2 5 10 μM
37 kD
75 kD
xCT
LaminB

Figure 3.2. Proteasome inhibitor induces xCT expression in a Nrf2- and ATF4-dependent manner. (A) T24 cells were exposed to 50 or 100 nM BTZ or EPO or 5 mM MG132 for 6 h, and Nrf2 and ATF4 protein expression levels were analyzed by immunoblot analysis. (B) T24 cells were exposed to 20 nM BTZ for 1 to 24 h, and eIF2α phosphorylation, ATF4 and Nrf2 protein expressions were assessed by immunoblot analysis. (C) *Nrf2* and *ATF4* mRNA expression by 20 nM BTZ were evaluated by RT-qPCR analysis. Differences between groups (vs. 0 h control) were assessed by one-way ANOVA with Bonferroni *post-hoc* test. $^{**}p<0.01$. (D) T24 cells were transfected with Nrf2 and/or ATF4 siRNAs as described in Materials and Methods. At 24 h post-transfection, the T24 cells were treated with DMSO (open bar), 20 nM BTZ (gray bar) or 100 nM bortezomib (black bar) for another 6 h and *xCT* mRNA expression was evaluated by RT-qPCR analysis. Differences between groups (vs. control siRNA) were assessed with one-way ANOVA/Bonferroni *post-hoc* test $^{**}p<0.01$. (E), (F) Immunoblot analysis of siRNA-transfected T24 cells. The arrowheads indicate Nrf2 or ATF4, and asterisks indicate nonspecific bands. (G) HeLa cells were exposed to tBHQ or Tm, as indicated in the figure for 24 h. Then, immunoblot analyses were performed to evaluate Nrf2 and ATF4 expression. (H) HeLa cells were treated with tBHQ and/or Tm as indicated for 24 h. *xCT* mRNA expression was analyzed by RT-qPCR and normalized with *CypA* expression. The data are presented as the means±SEM from at least three independent experiments. Differences between groups were assessed by one-way ANOVA with Bonferroni *post-hoc* test. $^{*}p<0.05$. (I), (J) xCT protein induction by tBHQ and/or Tm treatment (24 h) in T24 cells was analyzed by immunoblot analysis.

3.3 Nrf2 and ATF4 coordinately upregulate *xCT* gene expression.

One functional ARE and two AAREs have been identified in the mouse *xCT* gene promoter and are responsible for *xCT* gene expression (30, 31). Sequence data analysis revealed that these *cis*-elements are also conserved in the human *xCT* gene promoter (Fig. 3.3A). To investigate whether these ARE and AARE elements mediate BTZ-inducible xCT expression, we constructed a series of human *xCT* gene promoter-luciferase reporter constructs and analyzed responsiveness to BTZ (Fig. 3.3B, See Materials and Methods). As shown in Fig. 3.3B, the wild-type reporter gene (pxCT-pro WT-Luc) showed strong constitutive and BTZ-inducible reporter activity. However, both constitutive and BTZ-inducible reporter activities were decreased in the ARE mutant and the AARE double mutant reporter genes (mt1-Luc and mt2-Luc, respectively) (Fig. 3.3B). Notably, both constitutive and BTZ-inducible reporter activities were almost abolished when both the ARE and the two AAREs were mutated (mt3-Luc) (Fig. 3.3B). Ectopically expressed Nrf2 and ATF4 were also able to activate the wild-type reporter (Fig. 3.3C). When ARE was mutated (mt1-Luc), Nrf2 lost the ability to induce reporter gene activity, whereas ATF4 was still able to activate the reporter. Interestingly, although there is no Nrf2 binding site in the reporter construct, Nrf2 further activated ARE mt-Luc (mt1-Luc) in the presence of ATF4 (Fig. 3.3C). Similarly, the AARE double mutant reporter (mt2-Luc) was not activated by ATF4, but in the presence of Nrf2, ATF4 further activated reporter gene activity, although this difference was not significant (Fig. 3.3C). Neither Nrf2 nor ATF4 was able to activate the reporter when both ARE and the two AAREs were mutated (mt3-Luc) (Fig. 3.3C).

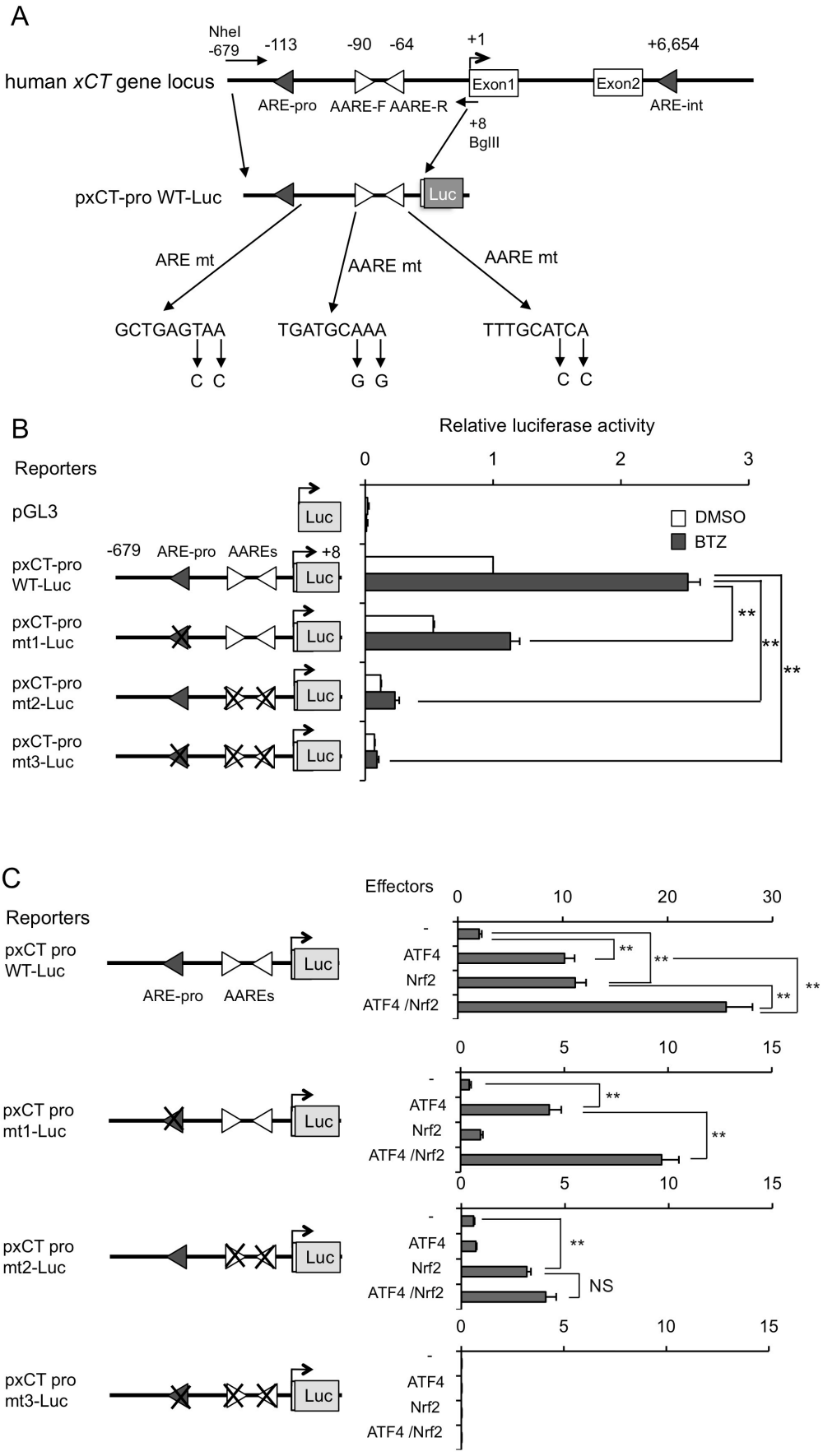
A
NheI
-679
-113
-90
-64
+1
+6,654
human xCT gene locus
Exon1
Exon2
ARE-pro
AARE-F
AARE-R
ARE-int
+8
BglII
pxCT-pro WT-Luc
Luc
ARE mt
AARE mt
AARE mt
GCTGAGTAA
TGATGCAAA
TTTGCATCA
C C
G G
C C
B
Relative luciferase activity
0
1
2
3
Reporters
pGL3
DMSO
BTZ
-679
ARE-pro
AAREs
+8
pxCT-pro WT-Luc
pxCT-pro mt1-Luc
pxCT-pro mt2-Luc
pxCT-pro mt3-Luc
**
C
Effectors
0
10
20
30
Reporters
pxCT pro WT-Luc
ARE-pro
AAREs
-
ATF4
Nrf2
ATF4 /Nrf2
pxCT pro mt1-Luc
pxCT pro mt2-Luc
pxCT pro mt3-Luc
NS

Figure 3.3. Reporter analysis of the human *xCT* gene promoter. (A) Schematic representation of human *xCT* gene locus and human *xCT* gene promoter-luciferase reporter. The putative ARE (ARE-pro) and the two AAREs (AARE-F and AARE-R) are indicated by closed and open triangles, respectively. Nucleotide substitutions in mutant reporters are described below. (B) T24 cells were transfected with either a wild-type reporter gene (pxCT pro WT-Luc) or mutated reporter genes and then incubated for 6 h in the presence of DMSO (open bar) or 100 nM BTZ (closed bar). Reporter activities were measured as described in Materials and Methods. (C) HeLa cells were cotransfected with each reporter plasmid in combination with the Nrf2 and/or ATF4 expression vectors. After 24 h of incubation, the transfected cells were subjected to the luciferase assay. Luciferase activities were normalized with Renilla luciferase activities, and the bars represent the means±SEM from at least three independent experiments. Differences between groups were assessed by one-way ANOVA with Bonferroni *post-hoc* test. *$p<0.05$, **$p<0.01$, NS: not significant.

In addition to above mentioned *cis*-elements in the human *xCT* gene promoter, we found a novel ARE consensus sequence in the second intron of the human *xCT* gene (6,654 nucleotides from transcription start site) by *in silico* analysis (Fig. 3.4A, See Materials and Methods). To investigate the function of this ARE sequence (named intronic ARE or ARE-int), we constructed WT and mutant reporter genes (Fig. 3.4A, See Materials and Methods). Interestingly, BTZ treatment and Nrf2 overexpression separately enhanced WT reporter activity but not mutant reporter activity (Fig. 3.4B and C). These results suggest that Nrf2 modulates human *xCT* gene expression not only through the promoter ARE but also through the intronic ARE.

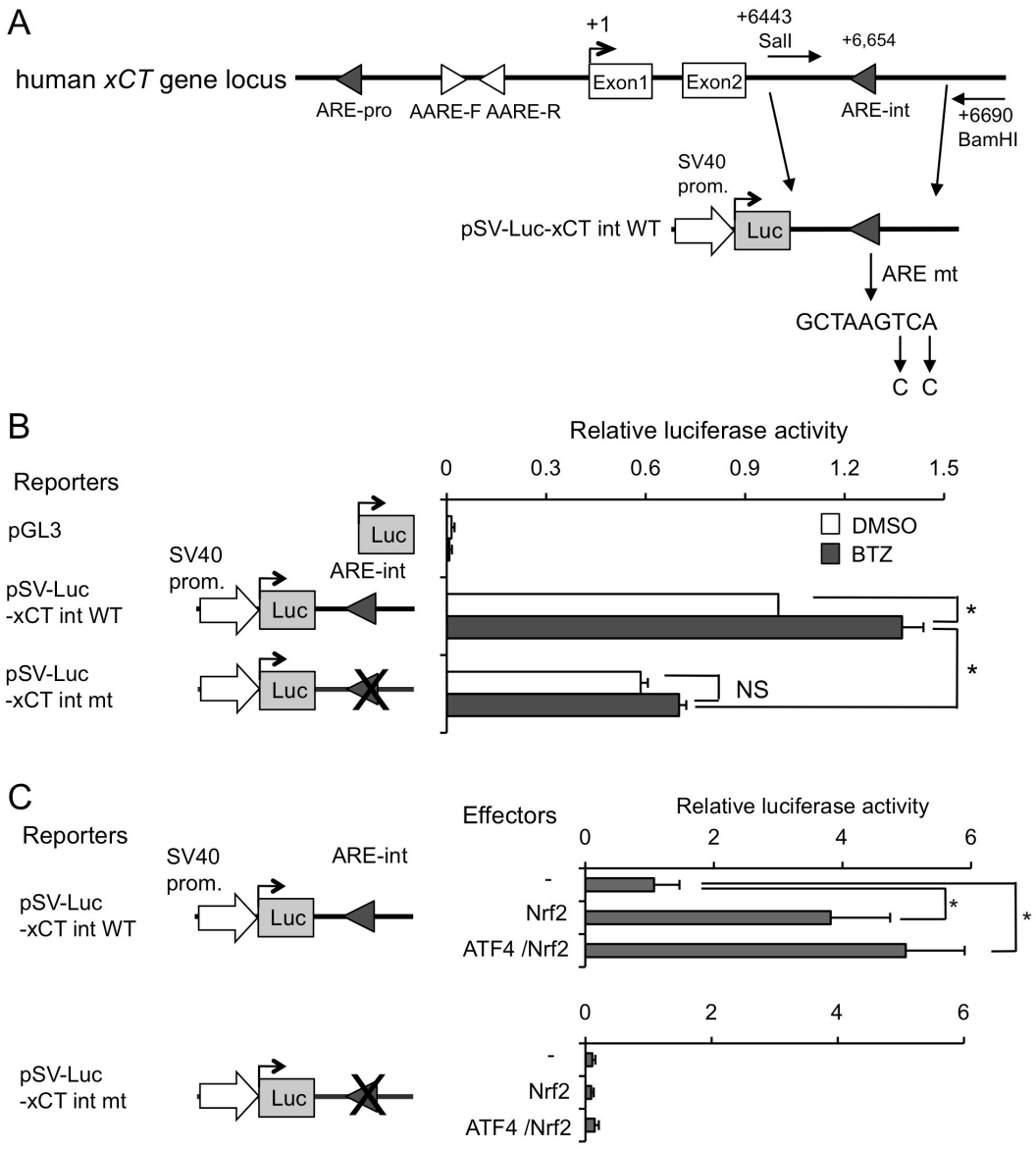

Figure 3.4. Reporter analysis of the human *xCT* gene intronic enhancer. (A) The construction of pSV-Luc-xCT int reporter WT and mutant. The putative ARE (ARE-int) is indicated by closed triangle. Nucleotide substitutions in mutant reporters are described below. (B) Reporter constructs containing a wild type or mutated intronic ARE were transfected into T24 cells and analyzed in the same manner as described for Fig. 3.3B. (C) Reporter constructs containing wild-type and mutant intronic ARE were cotransfected with a Nrf2 or ATF4 expression vector as described in Fig. 3.3C. Luciferase activities were normalized with Renilla luciferase activities, and the bars represent the means±SEM from at least three independent experiments. Differences between groups were assessed by one-way ANOVA with Bonferroni *post-hoc* test. *p<0.05, NS: not significant.

To evaluate Nrf2 or ATF4 recruitment to the human *xCT* gene in response to BTZ, we performed ChIP assays. The PCR-amplified regions used in the ChIP assay are shown in Fig. 3.5A. After BTZ treatment, both Nrf2 and ATF4 were recruited to the promoter region of the human *xCT* gene (Fig. 3.5B and C left panels), but neither Nrf2 nor ATF4 was recruited to the first intron region (negative control region) (Fig. 3.5B and C middle panels). Notably, Nrf2 bound to the ARE in the second intron upon BTZ treatment (Fig. 3.5B right panel). Interestingly, ATF4 was also recruited to the intronic ARE by BTZ, although there are no ATF4 binding sites in this region (Fig. 3.5C right panel). It is noteworthy that Nrf2 knockdown did not affect ATF4 recruitment to the promoter ARE, but it completely abolished ATF4 recruitment to the intronic ARE upon BTZ treatment (Fig. 3.5D). This ChIP result and reporter analysis result (Fig. 3.3C) strongly suggest that Nrf2 and ATF4 may interact during *xCT* gene regulation. As expected, Nrf2 and ATF4 interaction was observed by GST pull-down experiments (Fig. 3.5E to H). GST pull-down experiments also revealed that both C-terminal bZip and N-terminal transactivation domains of ATF4 associate with Nrf2 protein (Fig. 3.5E). On the other hand, C-terminal domain of Nrf2, which contains Cap'n'Color (CNC)-bZip and Nrf2-ECH-homology (Neh) 3 domains, conferred ATF4 interaction (Fig. 3.5F). These results indicate that Nrf2 and ATF4 physically interact to cooperatively activate human *xCT* gene expression upon BTZ treatment.

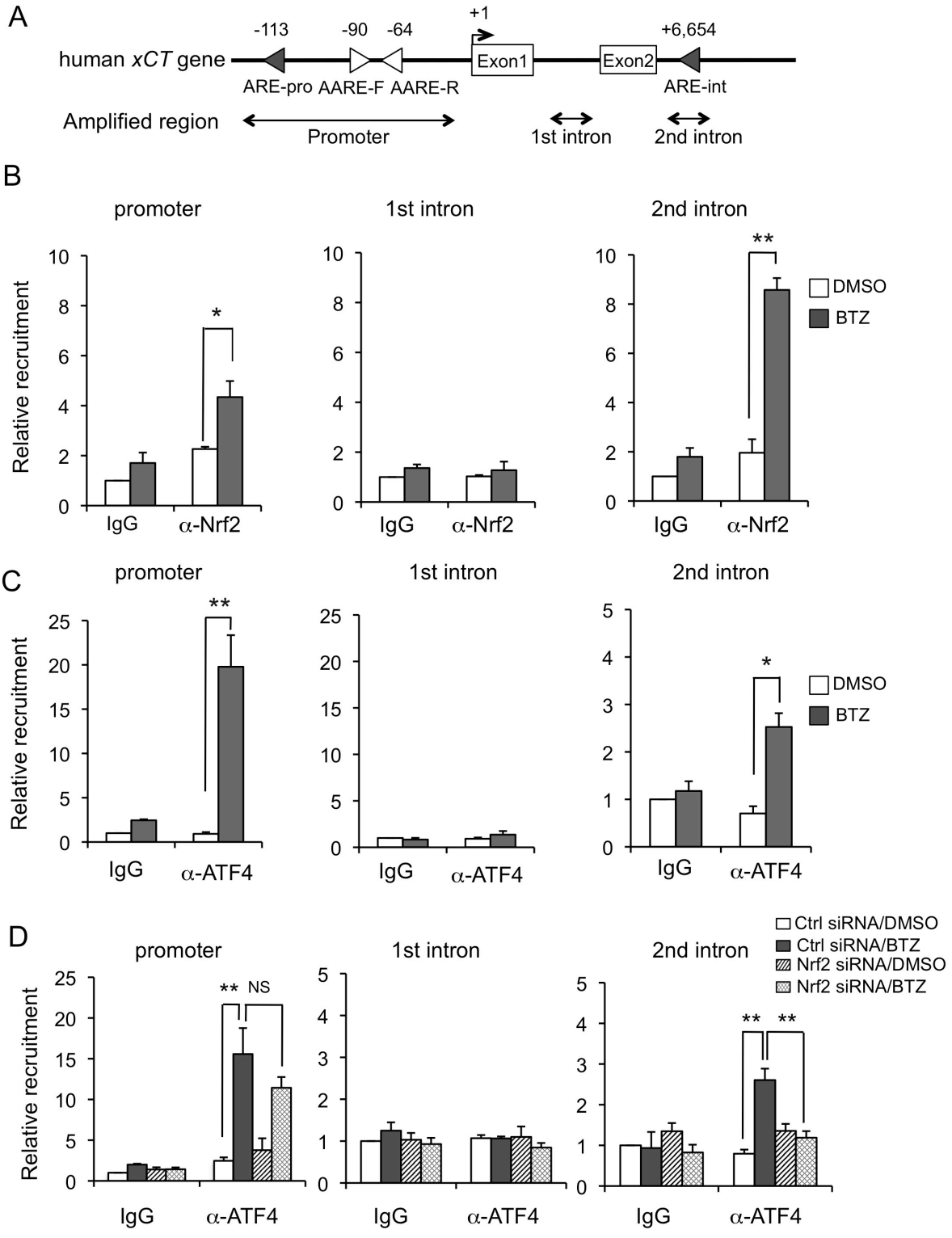
A
human xCT gene
-113
-90
-64
+1
+6,654
Exon1
Exon2
ARE-pro
AARE-F
AARE-R
ARE-int
Amplified region
Promoter
1st intron
2nd intron
B
promoter
1st intron
2nd intron
Relative recruitment
IgG
α-Nrf2
DMSO
BTZ
C
promoter
1st intron
2nd intron
Relative recruitment
IgG
α-ATF4
DMSO
BTZ
D
promoter
1st intron
2nd intron
Relative recruitment
NS
IgG
α-ATF4
Ctrl siRNA/DMSO
Ctrl siRNA/BTZ
Nrf2 siRNA/DMSO
Nrf2 siRNA/BTZ

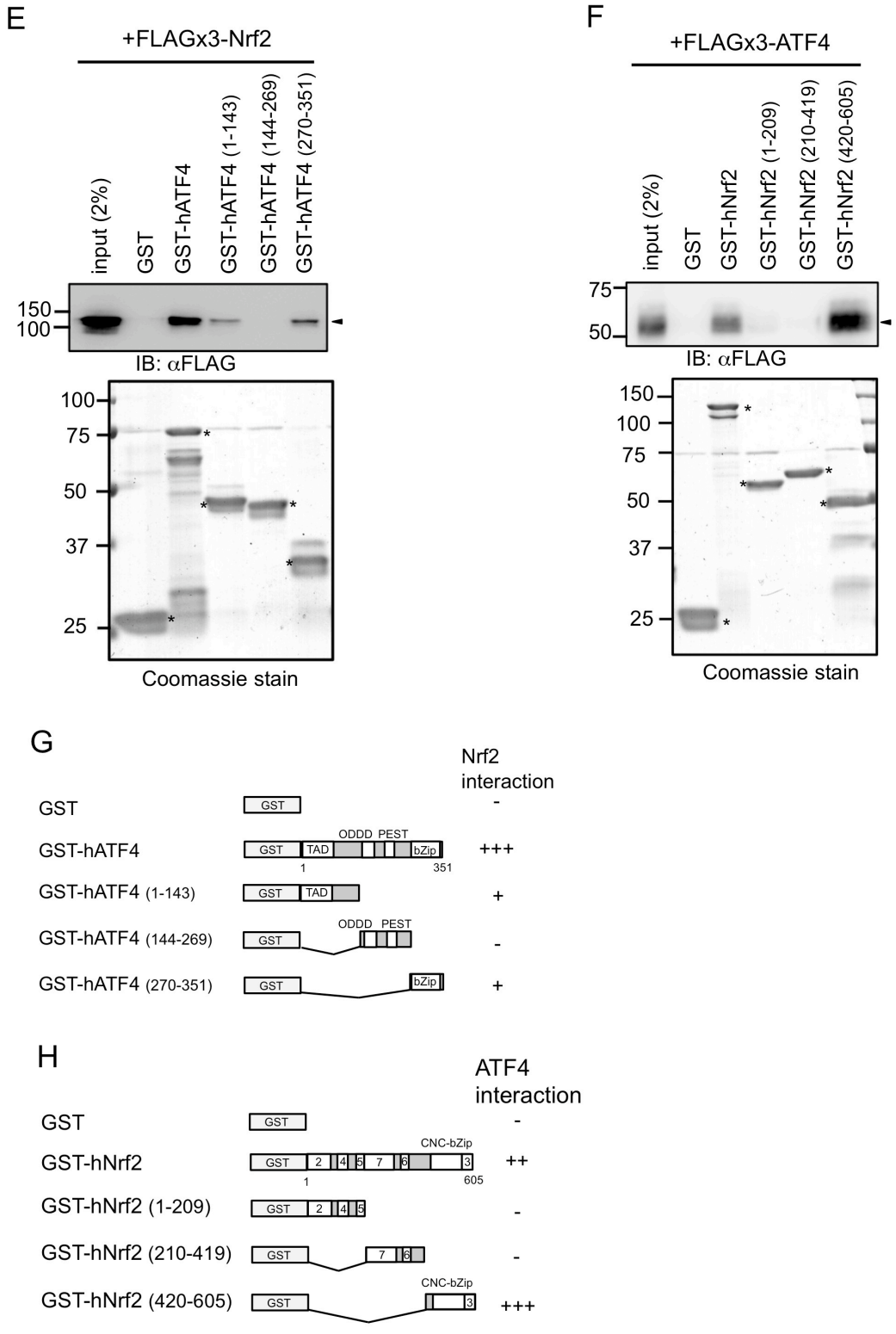

Figure 3.5. BTZ-induced Nrf2 and ATF4 recruitment to *cis*-regulatory elements of the human *xCT* gene. (A) Schematic representation of the human *xCT* gene locus and PCR-amplified regions used in the ChIP assay. (B), (C) T24 cells were treated with DMSO (open bar) or 100 nM BTZ (closed bar) for 6 h and subjected to a ChIP assay using anti-Nrf2 or anti-ATF4 antibodies as described in Materials and Methods. The first intron region was used as a negative control. (D) T24 cells were transfected with

control or Nrf2 siRNAs. At 24 h post-transfection, the cells were treated with 100 nM BTZ for 6 h and subjected to a ChIP assay using anti-ATF4 antibody. The data were expressed relative to the corresponding values for the DMSO-treated and normal IgG-captured fragment, and the data represent the means±SEM from at least three independent experiments. Differences between groups were assessed by one-way ANOVA with Bonferroni *post-hoc* test. *p<0.05, **p<0.01, NS: not significant. (E) Interaction between bacterially expressed GST-ATF4 fusion proteins and FLAG-tagged Nrf2 expressed in 293T cells were analyzed by GST pull-down experiment. GST-ATF4 bound FLAGx3-Nrf2 was detected by anti-FLAG antibody (upper panel), and GST-ATF4 fusion proteins were visualized by Coomassie staining (lower panel). The arrowhead indicates FLAG tagged Nrf2, and asterisks indicate GST or GST-Nrf2 fusion proteins. (F) Interaction between bacterially expressed GST-Nrf2 fusion proteins and FLAG-tagged ATF4 expressed in 293T cells were assessed by GST pull-down experiment. GST-Nrf2 bound FLAGx3-ATF4 was detected by anti-FLAG antibody (upper panel), and GST-Nrf2 fusion proteins were visualized by Coomassie staining (lower panel). The arrowhead indicates FLAG tagged ATF4, and asterisks indicate GST or GST-ATF4 fusion proteins. (G), (H) Schematic representation of GST-ATF4 fusion proteins and GST-Nrf2 fusion proteins used in pull-down experiment. The numbers of schematic Nrf2 molecule indicate Neh domain 1-7.

3.4 xCT inhibition increases bortezomib sensitivity.

To investigate whether upregulated xCT affects the BTZ sensitivity of T24 cells, we next suppressed xCT function by using xCT siRNA or pharmacologic xCT inhibitors. As shown in Fig. 3.6D, the constitutive and BTZ-inducible xCT expression levels were effectively decreased by xCT siRNA. Intriguingly, enhanced sensitivity to BTZ was observed in xCT-knockdown cells compared to control cells (Fig. 3.6A). Similarly, 6 h pretreatment with pharmacologic xCT inhibitor SASP (41) significantly enhanced BTZ sensitivity of T24 cells without affecting xCT induction by BTZ (Fig. 3.6B and E). In addition, this sensitization was abolished by cotreatment with 2-ME, which bypasses cystine transport by reducing extracellular cystine to cysteine and allowing the cellular uptake of cysteine via neutral amino acid transporters (Fig. 3.6B) (42). Another xCT inhibitor CPG also enhanced BTZ sensitivity (Fig. 3.6C). These results indicate that xCT has a protective role against BTZ-induced cytotoxicity in T24 cells.

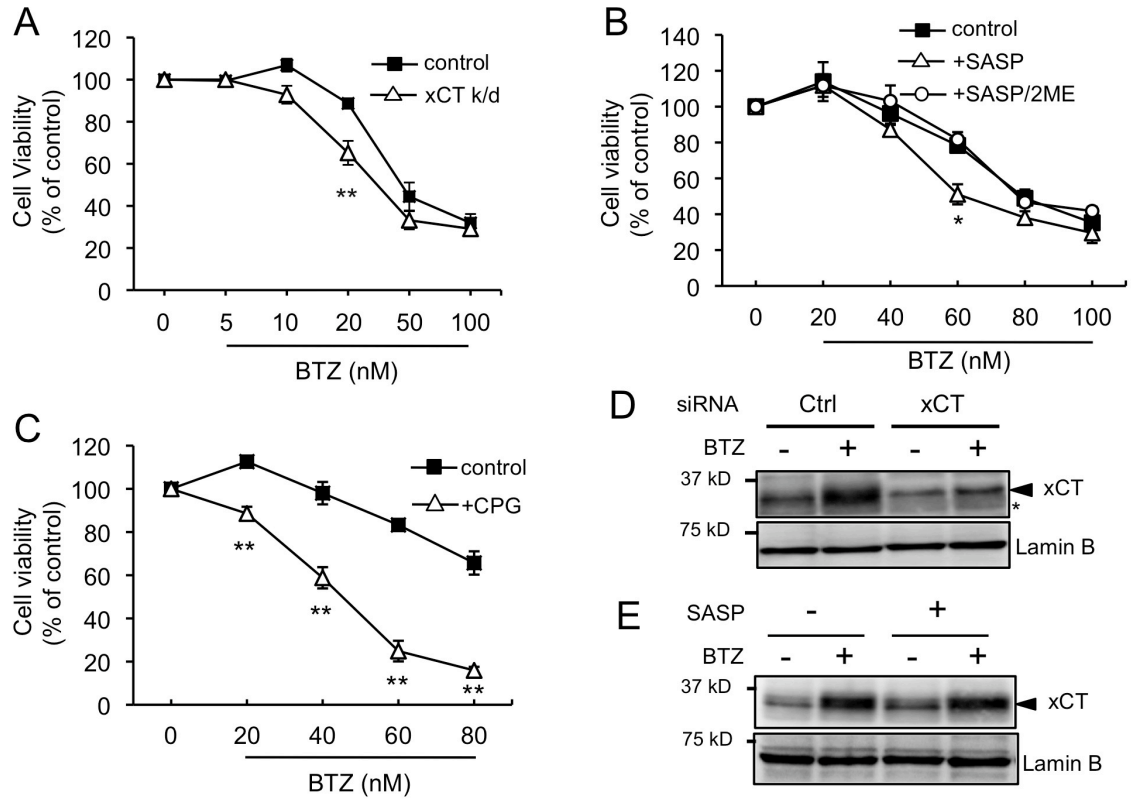

Figure 3.6. xCT knockdown by siRNA and xCT inhibitors sensitize T24 cells to BTZ. (A) T24 cells were transfected with either control (filled circle) or xCT siRNA (open triangle). At 24 h post-transfection, the cells were re-seeded on 96-well plates. After 24 h incubation, the cells were exposed to different concentrations of BTZ for 48 h, and cell viability was analyzed using CCK-8. The data are the means±SEM from at least three independent experiments. Differences between groups (vs. control) were assessed by one-way ANOVA with Bonferroni *post-hoc* test. **p*<0.05, ***p*<0.01. (B), (C) T24 cells were pre-treated with of 0.3 mM SASP in the presence or absence of 66 μM 2-ME or 0.2 mM CPG for 6 h and then treated with 20 to 100 nM BTZ for another 48 h. Cell viability was measured by using CCK-8. The data are expressed as the means±SEM from at least three independent experiments. Differences between groups (vs. respective control) were assessed by one-way ANOVA with Bonferroni *post-hoc* test. **p*<0.05, ***p*<0.01. (D) T24 cells were transfected with control or xCT siRNAs. After 24 h, the cells were treated with BTZ for 6 h and then subjected to immunoblot analysis. The arrowhead indicates xCT, and asterisk indicates nonspecific bands. (E) The effect of SASP on BTZ-induced xCT protein expression was assessed by immunoblot analysis.

Because xCT is crucial for the maintenance of intracellular cysteine and GSH levels, we analyzed intracellular cysteine and GSH levels in cells with xCT knocked down. BTZ treatment increased the intracellular cysteine level approximately 2-fold in control cells. However, the intracellular cysteine level was not increased in xCT-knockdown cells (Fig. 3.7A). Similarly, the cellular GSH level was increased by BTZ treatment and significantly decreased in xCT-knockdown cells (Fig. 3.7B). Nearly the same effects were observed in SASP treated T24 cells, although SASP more severely decreased intracellular GSH level (Fig. 3.7C and D). We next analyzed the effect of the antioxidant NAC on BTZ-induced cytotoxicity, because NAC is an antioxidant itself and functions as a source of cysteine and GSH (43). Interestingly, BTZ-induced cytotoxicity was attenuated by NAC in a dose-dependent manner (Fig. 3.7E). These results indicate that BTZ treatment decreases T24 cell viability in part through oxidative stress, and upregulated xCT attenuates oxidative stress by increasing the intracellular cysteine and GSH levels.

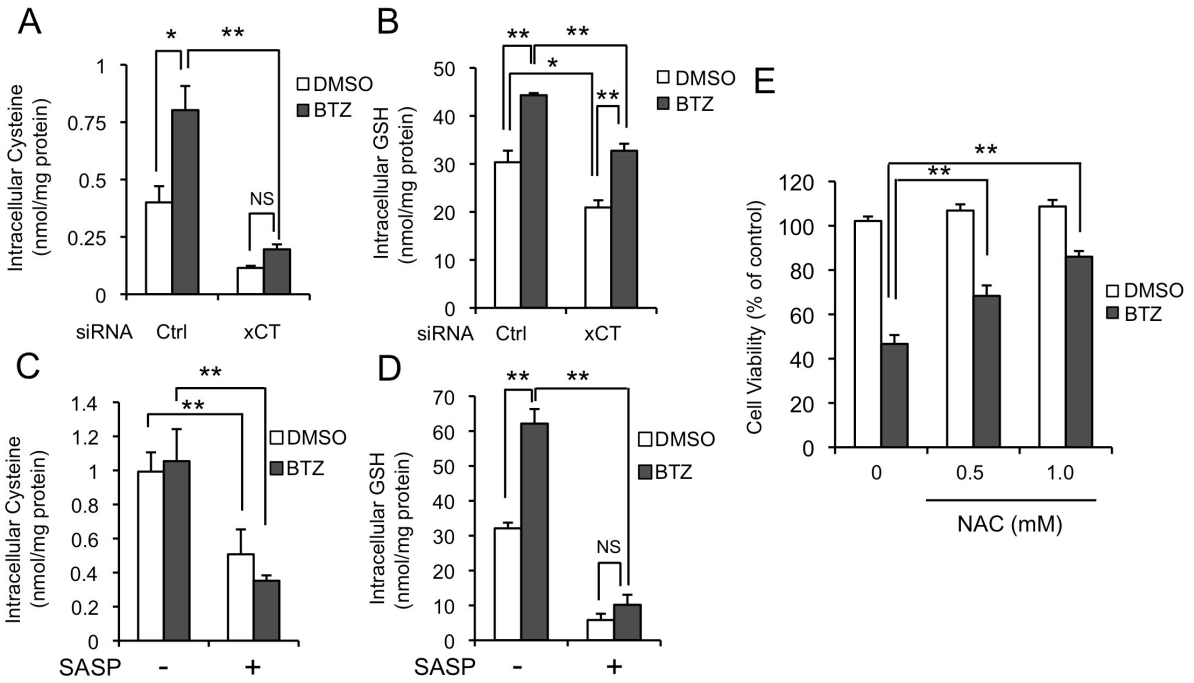

Figure 3.7. xCT knockdown or SASP treatment decrease intracellular cysteine and GSH levels. (A), (B) Intracellular cysteine and GSH levels in control or xCT siRNA-transfected T24 cells. 24 h after siRNA transfection, the cells were exposed to DMSO (open bar) or 20 nM BTZ (closed bar) for 18 h, and then cellular cysteine and GSH levels were measured as described in Materials and Methods. (C), (D) T24 cells were pretreated with 0.3 mM SASP for 6 h, then incubated in the presence or absence of 20 nM BTZ for another 24 h. Intracellular cysteine and GSH levels were analyzed as described above. (E) T24 cells were pretreated with 0.5 or 1 mM NAC for 30 min and then treated with 100 nM BTZ. After 48 h of incubation, cell viability was measured. The value of untreated cells was arbitrarily set as 100 % and the means of relative values were presented with SEM. Differences between groups were assessed by one-way ANOVA with Bonferroni *post-hoc* test. *p<0.05, **p<0.01, NS: not significant.

3.5 xCT knockdown or SASP generally increase the sensitivity of T24 cells to proteasome inhibitors.

To investigate whether xCT inhibition affects cytotoxic effect of proteasome inhibitors other than BTZ, we next analyzed the effect of xCT inhibition on EPO-, MG132- and CFZ-induced cytotoxicity in T24 cells. As shown in Fig. 3.8A and B, xCT knockdown and SASP significantly increased the EPO sensitivity of T24 cells. SASP did not affect the inducibility of xCT by EPO (Fig. 3.8C). In addition, cytotoxic effects of MG132 and CFZ also increased by SASP treatment (Fig. 3.8D and E). The cytotoxicities of these proteasome inhibitors were also enhanced by CPG in T24 cells (Fig. 3.8F and G). These results indicate that xCT generally protects T24 cells from cytotoxic effect of proteasome inhibitors.

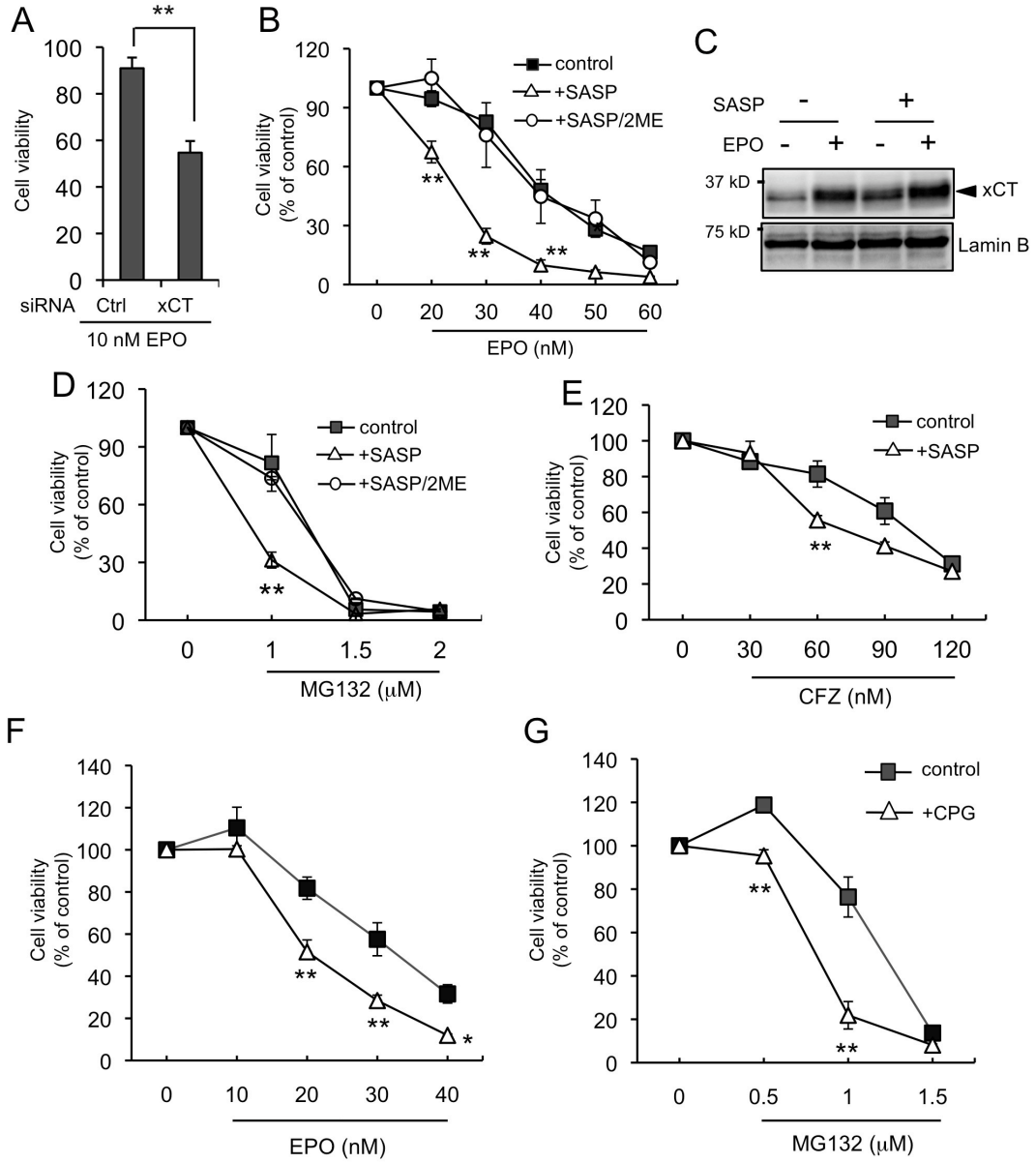

Figure 3.8. Effects of xCT inhibition on T24 cell sensitivity to other proteasome inhibitors. (A) T24 cells were transfected with xCT siRNA as described in Fig. 6A, and then treated with 10 nM EPO. Cell viability was evaluated after 48 h by using CCK-8. (B) T24 cells were pretreated with 0.3 mM SASP in the presence or absence of 66 μM 2-ME for 30 min and then exposed to 20 to 60 nM EPO. After 48 h of incubation, cell viability was measured using CCK-8. (C) The effect of SASP on EPO-induced xCT expression was assessed by immunoblot analysis. The arrowhead indicates xCT. (D), (E) T24 cells were pretreated with 0.3 mM SASP for 30 min and then treated with different concentrations of MG132 or CFZ. After 48 h incubation, cell viability was measured as described above. The data were expressed relative to the corresponding value for untreated cells. (F), (G) T24 cells were pretreated with 0.2 mM CPG and then treated with different concentrations of EPO or MG132. After 48 h incubation, cell viability was measured as described above. Differences between groups (vs. respective control) were assessed by one-way ANOVA with Bonferroni *post-hoc* test. $^{**}p<0.01$.

3.6 xCT knockdown increases BTZ sensitivity of other cancer cell lines.

It is unknown whether xCT affects BTZ sensitivity in other cancer cell lines except for T24 cells. By using T98G glioblastoma and U373MG astrocytoma cells, we found that xCT was induced by BTZ treatment and xCT knockdown increased BTZ sensitivity (Fig. 3.9A to D). However, several cancer cells, such as HeLa and MCF7, were severely damaged by xCT knockdown only and we were not able to assess the effect of xCT knockdown on BTZ sensitivity (data not shown). These results indicate that xCT may generally affect cancer cell survival under normal and stressed conditions. On the other hand, several other genes, such as *HSPA2/Hsp72*, *PSMB5* and *BIRC5/survivin*, have been shown to decrease BTZ sensitivity in several cancer cells (10, 14, 44). To investigate whether BTZ induces these genes in T24 cells, we analyzed these gene expressions. RT-qPCR analysis revealed that all of genes except for *PSMB5* are increased by BTZ treatment (Fig. 3.9E). In addition, expressions of *GCLC* and glutamate-cysteine ligase modulatory subunit (*GCLM)*, which increase cellular GSH biosynthesis, were also upregulated by BTZ treatment (Fig. 3.9E). These results indicate that several genes other than xCT may also contribute to T24 cell survival during proteasome inhibition.

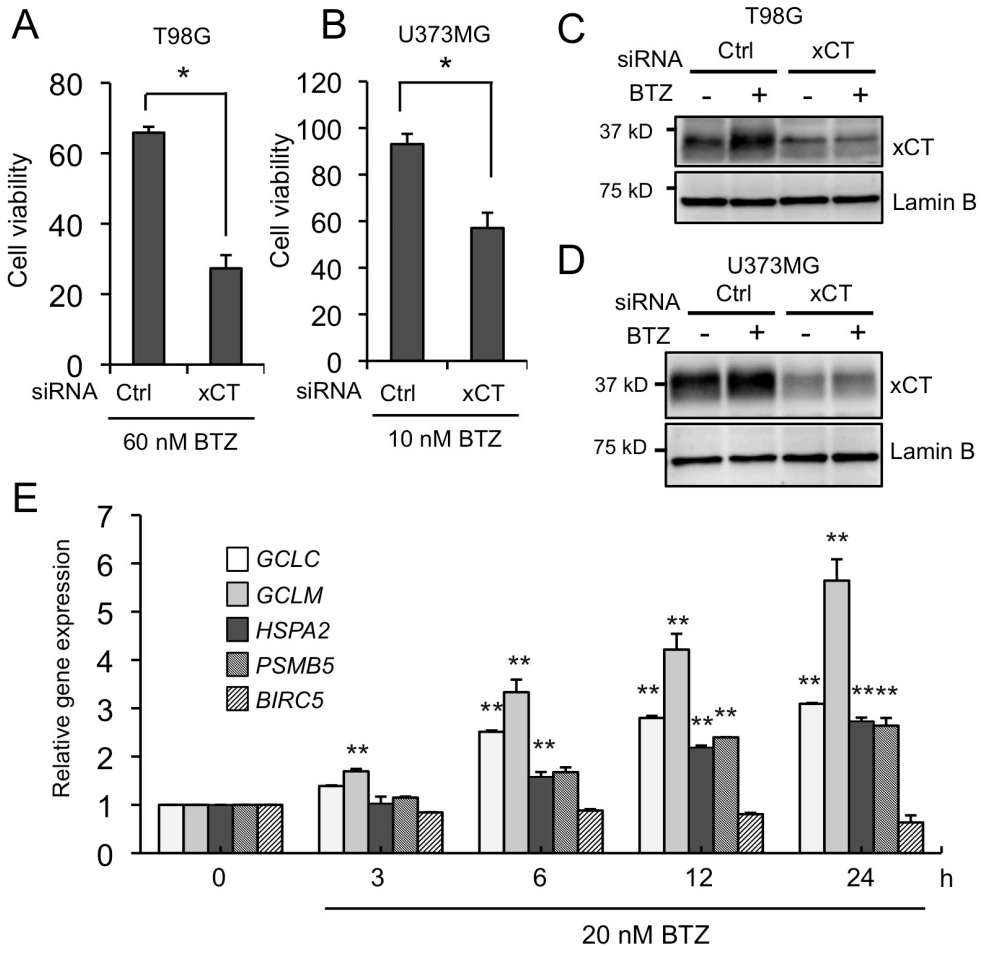

Figure 3.9. xCT knockdown increases BTZ sensitivity of other cancer cell lines. (A), (B) Cell viability of xCT siRNA transfected T98G and U373MG cells after 48 h BTZ treatment. The data represent means±SEM from three independent experiments. Differences between groups were assessed with Student's *t*-test ***p*<0.01. (C), (D) T98G or U373MG cells were transfected with either control or xCT siRNA. After 24 h transfection, the cells were exposed to BTZ for 6 h and the whole cell lysates were subjected to immunoblot analysis. (E) T24 cells were treated with 20 nM BTZ for 3 to 24 h, and then *GCLC, GCLM, HSPA2, PSMB5* and *BIRC5* mRNA expression was evaluated by RT-qPCR and normalized with CypA expression levels. The data represent means±SEM from three independent experiments. Differences between groups (vs. respective 0 h control) were assessed with one-way ANOVA/Bonferroni *post-hoc* test, ***p*<0.01.

4 Discussion

In bladder cancer treatment, many cytotoxic, anti-angiogenic, epigenetic agents have been tested in chemotherapy (16-19). To increase the efficacy of anti-cancer drugs, it is important to understand what types of mechanisms confer chemoresistance to tumor cells. In this study, we revealed the role of xCT in T24 sensitivity to proteasome inhibitors, and the molecular mechanisms by which proteasome inhibitors induce xCT are summarized in Fig. 4.1. Because of its fundamental importance in cellular processes, the proteasome has been considered a promising target of anti-cancer chemotherapy (5, 6). Many types of proteasome inhibitors have been developed, and some of them have been approved as anti-cancer drugs or currently undergoing phase II or III trials. BTZ is the first proteasome inhibitor approved for clinical treatment (5-7). BTZ shows cytotoxic effects in many cancer cells, including myeloma, mantle cell lymphoma, head and neck carcinoma and bladder cancer cells. However, similar to other anti-cancer drugs, intrinsic and acquired resistance to BTZ were observed (9). For example, BIRC5/survivin expression and p53 status affect BTZ sensitivity in several cancer cell lines (14). BTZ-induced HSPA2/HSP72 protects human bladder carcinoma cells from BTZ-induced cell death (10). Mutations in the proteasome subunit PSMB5 and PSMB5 overexpression confer BTZ resistance in human myelomonocytic THP1 cells (44). The up-regulation of the insulin-like growth factor-1 signaling pathway also affects BTZ resistance in multiple myeloma (45). As shown in Fig. 3.9E, HSPA2 and PSMB5 were upregulated by BTZ indicating the possibility that these genes affect BTZ cytotoxicity in T24 cells. These data emphasize the importance of clarifying the cellular pathway that

affects the efficacy of BTZ in cancer cells.

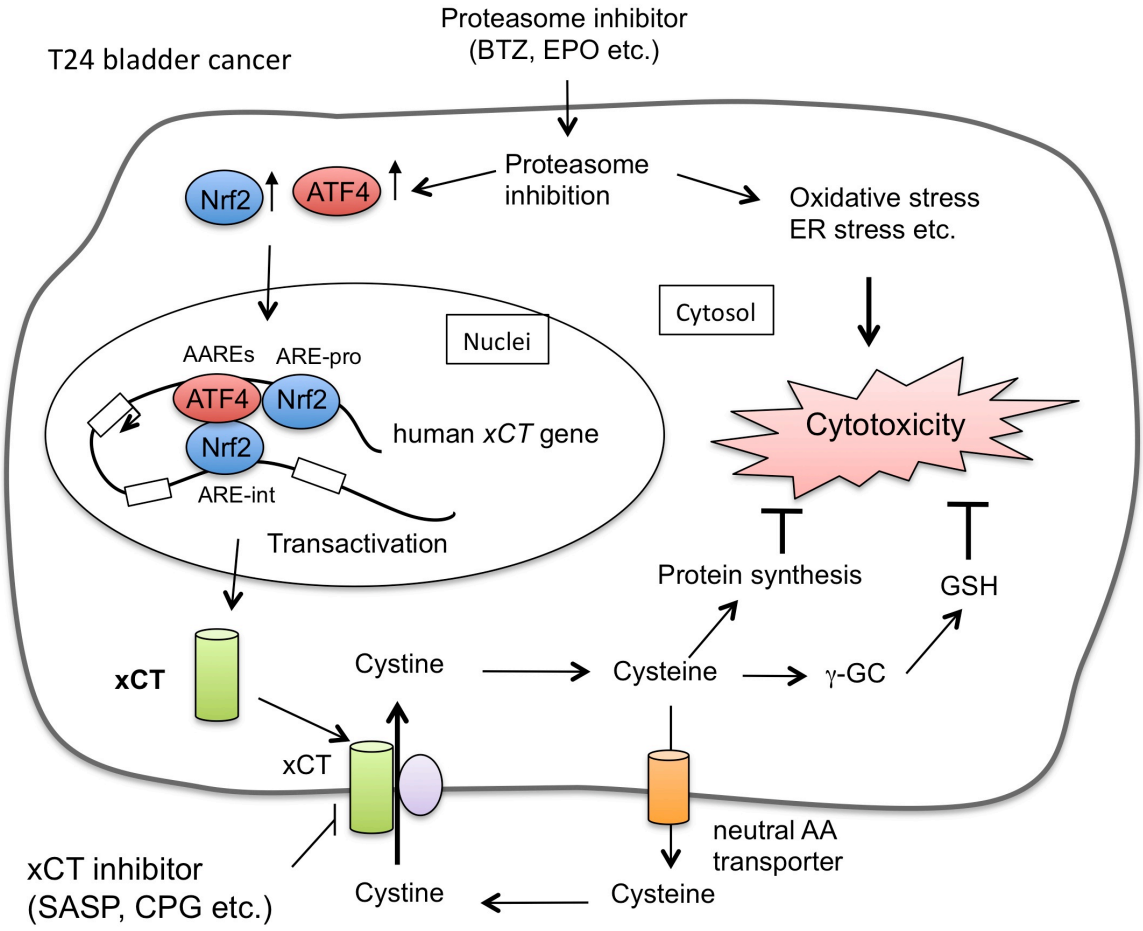

Figure 4.1. Hypothetical model for xCT induction by proteasome inhibitors and its effect on proteasome inhibitor-induced cytotoxicity in T24 cells. Proteasome inhibitor-induced xCT protects the cells from the cytotoxic effects of the proteasome inhibitor. See details in the text.

xCT has been considered a potential target of cancer treatment. The pharmacological inhibition of xCT function by SASP disrupts the proliferation of lymphoma, glioma, prostate cancer and hepatocellular carcinoma (41, 46, 47, 48). It was also reported that xCT inhibition represses esophageal cancer cell metastasis and that both siRNA-mediated xCT knockdown and SASP treatment induce autophagic cell death in hepatocellular carcinoma (48, 49). Because xCT is highly induced by BTZ

treatment and because xCT knockdown by siRNA increases the BTZ cytotoxicity of T24 cells (Fig. 3.6D), we conclude that xCT is one of the mediators of BTZ resistance in T24 cells. In hepatocellular carcinoma, xCT inhibition abrogates GSH synthesis and increases ROS (48). In our experiments, xCT knockdown and SAPS pretreatment decrease intracellular cysteine and GSH levels (Fig. 3.7A to D). These results indicate the association between BTZ cytotoxicity and oxidative stress. The attenuation of BTZ cytotoxicity by NAC co-treatment supports this idea (Fig. 3.7E). However, since GSH decline was not so severe in xCT knockdown, it is possible that BTZ-induced Nrf2 and ATF4 maintain intracellular GSH levels even in the absence of xCT because Nrf2 and ATF4 coordinately modulate the expression of many genes involved in the glutathione synthetic pathway, except for xCT (50). Further analysis is required to clarify the correlation between BTZ-induced xCT and GSH synthesis. Considering that xCT attenuates oxidative stress through creating a reducing extracellular environment via cystine/cysteine cycle upregulation, the xCT-dependent, but GSH-independent, antioxidative system may also affect the BTZ resistance of T24 cells (23, 51).

SASP is a sulfa drug used for the treatment of inflammatory bowel diseases and rheumatoid arthritis, and it is also a potent x_c^- inhibitor (41). A metabotropic glutamate receptor agonist/antagonist CPG also functions as an inhibitor of x_c^- (52). In T24 cells, SASP or CPG pretreatment increased BTZ sensitivity (Fig. 3.6B and C). Although 6 h SASP or CPG pretreatment were required for BTZ sensitization, only 30 min SASP pretreatment was sufficient to increase sensitivity to other proteasome inhibitors in T24 cells (Fig. 3.8 and data not shown). Currently, it is unknown what makes this

difference between BTZ and other proteasome inhibitors, however, cotreatment with these xCT inhibitors might improve proteasome inhibitor-based cancer chemotherapy. The FDA approved CFZ, a derivative of EPO, for the treatment of multiple myeloma in 2012 (53). Further studies are required to understand the effective drug combinations that simultaneously target xCT and the proteasome.

The regulation mechanisms of mouse *xCT* gene promoter by Nrf2 or ATF4 are well established and one ARE and two AAREs in promoter region are responsible for Nrf2 and ATF4 binding, respectively (30, 31). In this study, we found a novel Nrf2 responsive ARE in the second intron of *xCT* gene, which is conserved among mammalian species (Fig. 3.4). The evidences that ARE mutated *xCT* gene promoter-luciferase construct was strongly activated by ATF4 and Nrf2 co-expression (Fig. 3.3C) and BTZ-induced ATF4 recruitment to intronic ARE was diminished by Nrf2 knockdown (Fig. 3.5D) indicate that Nrf2 and ATF4 interact each other and cooperatively activate BTZ-induced *xCT* gene expression. He *et al.* reported that Nrf2/ATF4 heterodimer binds to stress-response element (StRE) of *HO-1* gene enhancer and activates StRE-dependent transcription (54). To bind StRE, Nrf2 and ATF4 likely interact through each bZip domains. In accordance with this, each C-terminal regions of Nrf2 and ATF4, which contains bZip domain, conferred interaction between Nrf2 and ATF4 (Fig. 3.5E and F). However, ATF4 transactivation domain also associated with Nrf2 (Fig. 3.5E). Since ATF4 activation domain contains second leucine zipper (L-Zip), it is possible that this second L-Zip domain interacts with Nrf2 bZip domain. It is also possible that ATF4 and Nrf2 interact indirectly through coactivators, because Nrf2 C-terminal region contains Neh3 transactivation domain (55). Further study is required to

clarify what kinds of Nrf2-ATF4 interaction regulate xCT gene induction.

Both Nrf2 and ATF4 play crucial roles in cancer cell survival and growth (36, 56-59). Nrf2 activates the antioxidative pathway by inducing a variety of antioxidant proteins in addition to xCT. In addition, Nrf2 upregulates phase II and phase III drug-metabolizing enzymes, which enhance the excretion of anti-cancer drugs from cancer cells (34, 35). Nrf2 also activates cancer cell growth through metabolic reprogramming (58). ATF4 is involved in many stress pathways including amino acid metabolism, redox homeostasis and ER stress response (37, 38). Because most of these stresses are unfavorable for cancer cells, ATF4 plays an important role in cancer cell growth and survival. Further, ATF4 increases chemoresistance in hepatocellular carcinoma (59). It is likely that other cytoprotective pathways driven by the Nrf2 or ATF4 pathways, such as *GCLC* and *GCLM*, also contribute to the resistance of T24 cells to BTZ. Further studies are needed to clarify this issue.

The present study has revealed that xCT induction confers resistance to T24 bladder carcinoma cells upon proteasome inhibition. It is plausible that cotreatment with an xCT inhibitor may improve proteasome inhibitor efficacy in bladder cancer chemotherapy.

Acknowledgements

I would like to thank Professor Ken Itoh and Dr. Junsei Mimura for offering me this occasion to accomplish this intriguing PhD project under their supervisions. I sincerely appreciate for their scientific support and vital guidance over the last three years. I studied a wide variety of research skills, which are important for my future research and career.

I also would like to appreciate Professor Hideyo Sato and Ms. Tomomi Okada for technical support and critical comments. I want to acknowledge Dr. Atsushi Maruyama and Dr. Tao Liu for their frank advice and valuable suggestions. I thank Professor Chikara Ohyama for kindly offering the bladder carcinoma cell lines. I thank Ms. Fumiko Tsukidate for technical assistance.

Finally, I am deeply grateful to my parents from the bottom of my heart for the understanding and support even though they are far away in China.

References

1. **Hochstrasser M.** 1995. Ubiquitin, proteasomes, and the regulation of intracellular protein degradation. Curr. Opin. Cell Biol. 7:215–223.

2. **Jentsch S, Schlenker S.** 1995. Selective protein degradation: a journey's end within the proteasome. Cell 82:881–884.

3. **Adams J.** 2003. The proteasome: structure, function, and role in the cell. Cancer Treat. Rev. 29 Suppl 1:3–9.

4. **Voorhees PM, Dees EC, O'Neil B, Orlowski RZ.** 2003. The proteasome as a target for cancer therapy. Clin. Cancer Res. 9:6316–6325.

5. **Adams J.** 2004. The development of proteasome inhibitors as anticancer drugs. Cancer Cell 5:417–421.

6. **Orlowski RZ, Kuhn DJ.** 2008. Proteasome inhibitors in cancer therapy: lessons from the first decade. Clin. Cancer Res. 14:1649–1657.

7. **Hideshima T, Richardson P, Chauhan D, Palombella VJ, Elliott PJ, Adams J, Anderson KC.** 2001. The proteasome inhibitor PS-341 inhibits growth, induces apoptosis, and overcomes drug resistance in human multiple myeloma cells. Cancer Res. 61:3071–3076.

8. **Kuhn DJ, Chen Q, Voorhees PM, Strader JS, Shenk KD, Sun CM, Demo SD, *et al.*** 2007. Potent activity of carfilzomib, a novel, irreversible inhibitor of the ubiquitin-proteasome pathway, against preclinical models of multiple myeloma. Blood 110:3281–3290.

9. **Lü S, Wang J.** 2013. The resistance mechanisms of proteasome inhibitor bortezomib. Biomark Res 1:13.

10. **Qi W, White MC, Choi W, Guo C, Dinney C, McConkey DJ, Siefker-Radtke A.** 2013. Inhibition of inducible heat shock protein-70 (hsp72) enhances bortezomib-induced cell death in human bladder cancer cells. PLoS ONE 8:e69509.

11. **Papageorgiou A, Kamat A, Benedict WF, Dinney C, McConkey DJ.** 2006. Combination therapy with IFN-alpha plus bortezomib induces apoptosis and inhibits angiogenesis in human bladder cancer cells. Mol. Cancer Ther. 5:3032–3041.

12. **Lashinger LM, Zhu K, Williams SA, Shrader M, Dinney CPN, McConkey DJ.** 2005. Bortezomib abolishes tumor necrosis factor-related apoptosis-inducing ligand resistance via a p21-dependent mechanism in human bladder and prostate cancer cells. Cancer Res. 65:4902–4908.

13. **Codony-Servat J, Tapia MA, Bosch M, Oliva C, Domingo-Domenech J, Mellado B, Rolfe M, *et al.*** 2006. Differential cellular and molecular effects of bortezomib, a proteasome inhibitor, in human breast cancer cells. Mol. Cancer Ther. 5:665–675.

14. **Ling X, Calinski D, Chanan-Khan AA, Zhou M, Li F.** 2010. Cancer cell sensitivity to bortezomib is associated with survivin expression and p53 status but not cancer cell types. J. Exp. Clin. Cancer Res. 29:8.

15. **Curran MP, McKeage K.** 2009. Bortezomib: a review of its use in patients with multiple

myeloma. Drugs 69:859–888.

16. **Ploeg M, Aben KKH, Kiemeney LA.** 2009. The present and future burden of urinary bladder cancer in the world. World J Urol 27:289–293.

17. **Siegel R, Naishadham D, Jemal A.** 2012. Cancer statistics, 2012. CA Cancer J Clin 62:10–29.

18. **Cote RJ, Datar RH.** 2003. Therapeutic approaches to bladder cancer: identifying targets and mechanisms. Crit. Rev. Oncol. Hematol. 46 Suppl:S67–83.

19. **Yang X, Flaig TW.** 2010. Novel targeted agents for the treatment of bladder cancer: translating laboratory advances into clinical application. Int Braz J Urol 36:273–282.

20. **Banjac A, Perisic T, Sato H, Seiler A, Bannai S, Weiss N, Kölle P, *et al.*** 2008. The cystine/cysteine cycle: a redox cycle regulating susceptibility versus resistance to cell death. Oncogene 27:1618–1628.

21. **Lu SC.** 2013. Glutathione synthesis. Biochim. Biophys. Acta 1830:3143–3153.

22. **Okuno S, Sato H, Kuriyama-Matsumura K, Tamba M, Wang H, Sohda S, Hamada H, *et al.*** 2003. Role of cystine transport in intracellular glutathione level and cisplatin resistance in human ovarian cancer cell lines. Br. J. Cancer 88:951–956.

23. **Sato H, Tamba M, Ishii T, Bannai S.** 1999. Cloning and expression of a plasma membrane cystine/glutamate exchange transporter composed of two distinct proteins. J. Biol. Chem. 274:11455–11458.

24. **Lewerenz J, Hewett SJ, Huang Y, Lambros M, Gout PW, Kalivas PW, Massie A, *et al.*** 2013.

The cystine/glutamate antiporter system x(c)(-) in health and disease: from molecular mechanisms to novel therapeutic opportunities. Antioxid. Redox Signal. 18:522–555.

25. **Lo M, Wang Y-Z, Gout PW.** 2008. The x(c)$^-$ cystine/glutamate antiporter: a potential target for therapy of cancer and other diseases. J. Cell. Physiol. 215:593–602.

26. **Huang Y, Dai Z, Barbacioru C, Sadée W.** 2005. Cystine-glutamate transporter SLC7A11 in cancer chemosensitivity and chemoresistance. Cancer Res. 65:7446–7454.

27. **Takeuchi S, Wada K, Toyooka T, Shinomiya N, Shimazaki H, Nakanishi K, Nagatani K, *et al.*** 2013. Increased xCT expression correlates with tumor invasion and outcome in patients with glioblastomas. Neurosurgery 72:33–41; discussion 41.

28. **Kinoshita H, Okabe H, Beppu T, Chikamoto A, Hayashi H, Imai K, Mima K, *et al.*** 2013. Cystine/glutamic acid transporter is a novel marker for predicting poor survival in patients with hepatocellular carcinoma. Oncol. Rep. 29:685–689.

29. **Ishimoto T, Nagano O, Yae T, Tamada M, Motohara T, Oshima H, Oshima M, *et al.*** 2011. CD44 variant regulates redox status in cancer cells by stabilizing the xCT subunit of system xc(-) and thereby promotes tumor growth. Cancer Cell 19:387–400.

30. **Sasaki H, Sato H, Kuriyama-Matsumura K, Sato K, Maebara K, Wang H, Tamba M, *et al.*** 2002. Electrophile response element-mediated induction of the cystine/glutamate exchange transporter gene expression. J. Biol. Chem. 277:44765–44771.

31. **Sato H, Nomura S, Maebara K, Sato K, Tamba M, Bannai S.** 2004. Transcriptional control of

cystine/glutamate transporter gene by amino acid deprivation. Biochem. Biophys. Res. Commun. 325:109–116.

32. **Zong Z-H, Du Z-X, Li N, Li C, Zhang Q, Liu B-Q, Guan Y, *et al.*** 2012. Implication of Nrf2 and ATF4 in differential induction of CHOP by proteasome inhibition in thyroid cancer cells. Biochim. Biophys. Acta 1823:1395–1404.

33. **Taguchi K, Tamba M, Bannai S, Sato H.** 2007. Induction of cystine/glutamate transporter in bacterial lipopolysaccharide induced endotoxemia in mice. J Inflamm (Lond) 4:20.

34. **Mitsuishi Y, Motohashi H, Yamamoto M.** 2012. The Keap1-Nrf2 system in cancers: stress response and anabolic metabolism. Front Oncol. 26:200.

35. **Itoh K, Mimura J, Yamamoto M.** 2010. Discovery of the negative regulator of Nrf2, Keap1: a historical overview. Antioxid. Redox Signal. 13:1665–1678.

36. **Taguchi K, Motohashi H, Yamamoto M.** 2011. Molecular mechanisms of the Keap1–Nrf2 pathway in stress response and cancer evolution. Genes Cells 16:123–140.

37. **Lewerenz J, Sato H, Albrecht P, Henke N, Noack R, Methner A, Maher P.** 2012. Mutation of ATF4 mediates resistance of neuronal cell lines against oxidative stress by inducing xCT expression. Cell Death Differ. 19:847–858.

38. **Ameri K, Harris AL.** 2008. Activating transcription factor 4. Int. J. Biochem. Cell Biol. 40:14–21.

39. **Kilberg MS, Shan J, Su N.** 2009. ATF4-dependent transcription mediates signaling of amino acid limitation. Trends Endocrinol. Metab. 20:436–443.

40. **Maruyama A, Mimura J, Harada N, Itoh K.** 2013. Nrf2 activation is associated with Z-DNA formation in the human HO-1 promoter. Nucleic Acids Res. 41:5223–5234.

41. **Gout PW, Buckley AR, Simms CR, Bruchovsky N.** 2001. Sulfasalazine, a potent suppressor of lymphoma growth by inhibition of the x(c)- cystine transporter: a new action for an old drug. Leukemia 15:1633–1640.

42. **Ishii T, Bannai S, Sugita Y.** 1981. Mechanism of growth stimulation of L1210 cells by 2-mercaptoethanol in vitro. Role of the mixed disulfide of 2-mercaptoethanol and cysteine. J. Biol. Chem. 256:12387–12392.

43. **Wo G. Fang YZ, Yang S, Lupton JR, Turner ND.** 2004. Glutathione Metabolism and Its Implications for Health. J. Nutr. 134:489-492.

44. **Oerlemans R, Franke NE, Assaraf YG, Cloos J, van Zantwijk I, Berkers CR, Scheffer GL, *et al.*** 2008. Molecular basis of bortezomib resistance: proteasome subunit beta5 (PSMB5) gene mutation and overexpression of PSMB5 protein. Blood 112:2489–2499.

45. **Kuhn DJ, Berkova Z, Jones RJ, Woessner R, Bjorklund CC, Ma W, Davis RE, *et al.*** 2012. Targeting the insulin-like growth factor-1 receptor to overcome bortezomib resistance in preclinical models of multiple myeloma. Blood 120:3260–3270.

46. **Chung WJ, Lyons SA, Nelson GM, Hamza H, Gladson CL, Gillespie GY, Sontheimer H.** 2005. Inhibition of cystine uptake disrupts the growth of primary brain tumors. J. Neurosci. 25:7101–7110.

47. **Doxsee DW, Gout PW, Kurita T, Lo M, Buckley AR, Wang Y, Xue H, *et al.*** 2007. Sulfasalazine-induced cystine starvation: potential use for prostate cancer therapy. Prostate 67:162–171.

48. **Guo W, Zhao Y, Zhang Z, Tan N, Zhao F, Ge C, Liang L, *et al.*** 2011. Disruption of xCT inhibits cell growth via the ROS/autophagy pathway in hepatocellular carcinoma. Cancer Lett. 312:55–61.

49. **Chen R-S, Song Y-M, Zhou Z-Y, Tong T, Li Y, Fu M, Guo X-L, *et al.*** 2009. Disruption of xCT inhibits cancer cell metastasis via the caveolin-1/beta-catenin pathway. Oncogene 28:599–609.

50. **Ehren JL, Maher P.** 2013. Concurrent regulation of the transcription factors Nrf2 and ATF4 mediates the enhancement of glutathione levels by the flavonoid fisetin. Biochem. Pharmacol. 85:1816–1826.

51. **Venè R, Castellani P, Delfino L, Lucibello M, Ciriolo MR, Rubartelli A.** 2011. The cystine/cysteine cycle and GSH are independent and crucial antioxidant systems in malignant melanoma cells and represent druggable targets. Antioxid. Redox Signal. 15:2439–2453.

52. **Gasol E, Jiménez-Vidal M, Chillarón J, Zorzano A, Palacín M.** 2004. Membrane topology of system xc- light subunit reveals a re-entrant loop with substrate-restricted accessibility. J. Biol. Chem. 279:31228-31236.

53. **Siegel DS.** 2013. From clinical trials to clinical practice: single-agent carfilzomib adverse events and their management in patients with relapsed and/or refractory multiple myeloma. Ther. Adv. Hematol. 4:354–365.

54. **He CH, Gong P, Hu B, Stewart D, Choi ME, Choi AM, Alam J.** 2001. Identification of activating transcription factor 4 (ATF4) as an Nrf2-interacting protein. Implication for heme oxygenase-1 gene regulation. J. Biol. Chem. 276:20858-20865.

55. **Nioi P, Nguyen T, Sherratt PJ, Pickett CB.** 2005. The Carboxy-Terminal Neh3 Domain of Nrf2 Is Required for Transcriptional Activation. Mol. Cell. Biol. 25:10895-10906.

56. **Singleton DC, Harris AL.** 2012. Targeting the ATF4 pathway in cancer therapy. Expert Opin. Ther. Targets 16:1189–1202.

57. **Mitsuishi Y, Motohashi H, Yamamoto M.** 2012. The Keap1-Nrf2 system in cancers: stress response and anabolic metabolism. Front Oncol. 2:200.

58. **Mitsuishi Y, Taguchi K, Kawatani Y, Shibata T, Nukiwa T, Aburatani H, Yamamoto M, *et al.*** 2012. Nrf2 redirects glucose and glutamine into anabolic pathways in metabolic reprogramming. Cancer Cell 22:66–79.

59. **Zhang Z, Yin J, Zhang C, Liang N, Bai N, Chang A, Liu Y, *et al.*** 2012. Activating transcription factor 4 increases chemotherapeutics resistance of human hepatocellular carcinoma. Cancer Biol. Ther. 13:435–442.